11-2021

Seasonality of Solute Flux and Water Source Chemistry in a Coastal Glacierized Watershed Undergoing Rapid Change: Wolverine Glacier Watershed, Alaska

Anna Bergstrom
Boise State University

Joshua C. Koch
U.S. Geological Survey

Shad O'Neel
U.S. Army Corps of Engineers

Emily Baker
U.S. Geological Survey

Water Resources Research

RESEARCH ARTICLE
10.1029/2020WR028725

Key Points:

- Electrical conductivity-discharge relationships indicate four hydroclimatic periods in a glacierized watershed
- Dominant source waters shift between hydroclimatic periods, particularly from snowmelt to groundwater
- Highest solute flux occurs during the late-season rainy period, which is projected to lengthen with changing climate

Supporting Information:

Supporting Information may be found in the online version of this article.

Correspondence to:

A. Bergstrom,
annabergstrom@boisestate.edu

Citation:

Bergstrom, A., Koch, J. C., O'Neel, S., & Baker, E. (2021). Seasonality of solute flux and water source chemistry in a coastal glacierized watershed undergoing rapid change: Wolverine Glacier watershed, Alaska. *Water Resources Research*, *57*, e2020WR028725. https://doi.org/10.1029/2020WR028725

Received 31 AUG 2020
Accepted 22 OCT 2021

Author Contributions:

Conceptualization: Anna Bergstrom, Joshua C. Koch
Data curation: Shad O'Neel, Emily Baker
Supervision: Anna Bergstrom, Joshua C. Koch, Shad O'Neel
Writing – review & editing: Anna Bergstrom, Joshua C. Koch, Shad O'Neel

Seasonality of Solute Flux and Water Source Chemistry in a Coastal Glacierized Watershed Undergoing Rapid Change: Wolverine Glacier Watershed, Alaska

Anna Bergstrom[1,2], Joshua C. Koch[3], Shad O'Neel[4], and Emily Baker[3]

[1]Department of Geosciences, Boise State University, Boise, ID, USA, [2]Institute of Arctic and Alpine Research, Boulder, CO, USA, [3]U.S. Geological Survey, Alaska Science Center, Anchorage, AK, USA, [4]U.S. Army Corps of Engineers, Hanover, NH, USA

Abstract As glaciers around the world rapidly lose mass, the tight coupling between glaciers and downstream ecosystems is resulting in widespread impacts on global hydrologic and biogeochemical cycling. However, a range of challenges make it difficult to conduct research in glacierized systems, and our knowledge of seasonally changing hydrologic processes and solute sources and signatures is limited. This in turn hampers our ability to make predictions on solute composition and flux. We conducted a broad water sampling campaign in order to understand the present-day partitioning of water sources and associated solutes in Alaska's Wolverine Glacier watershed. We established a relationship between electrical conductivity and streamflow at the watershed outlet to divide the melt season into four hydroclimatic periods. Across hydroclimatic periods, we observed a shift in nonglacial source waters from snowmelt-dominated overland and shallow subsurface flow paths to deeper groundwater flow paths. We also observed the shift from a low- to high-efficiency subglacial drainage network and the associated flushing of water stored subglacially with higher solute loads. We used calcium, the dominant dissolved ion, from watershed outlet samples to estimate solute fluxes for each hydroclimatic period across two melt seasons. We found between 40% and 55% of Ca^{2+} export occurred during the late season rainy period. This partitioning of the melt season coupled with a characterization of the chemical makeup and magnitude of solute export provides new insight into a rapidly changing watershed and creates a framework to quantify and predict changes to solute fluxes across a melt season.

1. Introduction

Glacierized watersheds play an important role in global hydrologic and biogeochemical cycles (e.g., Hood et al., 2015; Milner et al., 2017) and regional ecology (Cauvy-Fraunié & Dangles, 2019). For example, they sustain late-summer streamflow and maintain colder water temperatures relative to adjacent nonglacierized watersheds (Fellman et al., 2015; Hood & Berner, 2009; O'Neel et al., 2014). Glacierized watersheds also have high sediment and dissolved solute export due to high physical erosion rates (Anderson et al., 1997; Hallet et al., 1996). In some regions, glaciers are a major source of nutrients (Barnes et al., 2014; Baron et al., 2009; Saros et al., 2010) and carbon (Fellman et al., 2014; Hood et al., 2009; Hood & Scott, 2008). These characteristics structure downstream riverine and nearshore marine ecosystems, influencing species distributions and abundances (e.g., Arimitsu et al., 2016; Milner et al., 2017).

Relative to other ecosystems, the composition and magnitude of biogeochemical fluxes and controls glacierized watersheds exert on those fluxes are not well constrained. As a result, the direction and magnitude of change to solute and nutrient fluxes and ecosystem impacts is uncertain, and at times studies draw conflicting conclusions. This includes if glacierized watersheds are a source or sink of biogeochemically important solutes like carbon and nitrogen and whether they concentrate or dilute nutrient availability in the nearshore marine environment (e.g., Cantoni et al., 2020; Herman et al., 2013; McGovern et al., 2020; Torres et al., 2017; Tranter et al., 2002). One major reason for this uncertainty is the high temporal variability of streamflow and solute sources in a glacierized watershed (i.e., snow melt, tundra streams, subglacially stored water, ice melt, etc.) and our limited ability to access these locations and measure the full range of that variability (Krawczyk et al., 2003). Biogeochemical studies rely heavily on water sampling, which requires a physical presence at the study site; something that is not easily achieved in remote high mountain

or polar regions with extreme weather conditions. Frequently only water quantity is examined (e.g., Beamer et al., 2017; Valentin et al., 2018). When biogeochemical solute sources are considered, it is often for a short period of time or focused on diel cycles (e.g., Graly et al., 2017; Hindshaw et al., 2011).

Biogeochemical studies from glacierized watersheds show strong variability in nutrient and solute fluxes on diel to seasonal timescales (Dzikowski & Jobard, 2012; Fairchild et al., 1999; Hawkings et al., 2015; Hindshaw et al., 2011; Hood & Berner, 2009; Koch et al., 2010). Hydrologically, stream discharge timing and magnitude is typically dominated by snow and glacier melt and impacted by the configuration and efficiency of the subglacial drainage network, even with low percent glacier covered area (Fountain & Tangborn, 1985; Jansson et al., 2003). However, from a biogeochemical perspective, ice-free regions of glacierized basins can be important sources of solutes and nutrients, potentially influencing the water chemistry measured at the outlet (Hood & Berner, 2009). Seasonal ground thaw can be a strong control on whether runoff moves overland, through shallow, or deep subsurface flow pathways (Carey & Woo, 2001; Evans et al., 2018; Maclean et al., 1999) and thus on stream chemistry and runoff magnitude and timing (Koch et al., 2014; Maclean et al., 1999). Snowmelt and various terrestrial sources (i.e., shallow or deep groundwater, wetland, or forested areas) can also contribute to and affect observed stream biogeochemical signatures. The intersection of precipitation phase and timing, snow and ice melt, thaw of frozen ground and subglacial flow paths, and residence times in the sub- and nonglacier environment can result in highly variable stream water chemistry over the course of a season (Dahlke et al., 2014; Hindshaw et al., 2011; Liu et al., 2004).

Globally, glaciers are experiencing increasingly rapid mass loss (Zemp et al., 2015), with increases in summer temperatures as the dominant driver (Box et al., 2018; O'Neel et al., 2019; Zemp et al., 2019), and Alaska is particularly affected (Box et al., 2019; Chapin et al., 2014; Zemp et al., 2019). Projections through 2100 for glacier area loss in the Gulf of Alaska region range from 15% to 57% (Beamer et al., 2017; Huss & Hock, 2015; Marzeion et al., 2020). Warming is also altering precipitation regimes; with more precipitation occurring as rain and more rain-on-snow events, particularly in southeast Alaska and at low elevations (Mcafee et al., 2014; Littell et al., 2018). These changes are coincident with a total annual runoff increase by 9%–14% for the Gulf of Alaska region (Beamer et al., 2017; McGrath et al., 2017; Ziemen et al., 2016). Projections suggest that ice loss not only impacts the magnitude of runoff, but also that it will substantially change the timing of streamflow as well. We expect increased streamflow early in the season due to earlier onset of melt, and increased late-season streamflow, as more days are above freezing and precipitation falls as rain instead of snow (Beamer et al., 2017; O'Neel et al., 2014, 2015).

Given the diversity of water sources within glacierized basins, their rapid shifting with climate change, and that access to these watersheds is frequently limited, it is extremely challenging to measure the full range of geochemical signatures and fluxes from glacierized watersheds (Krawczyk et al., 2003), much less predict how these fluxes may change as ice cover diminishes in the future. We suggest that developing linkages between dominant water sources and hydrologic function of glacierized watersheds can help us better understand timing and mechanisms of solute export and serve as a platform for hypothesis testing regarding how these areas will change with further glacier mass loss. This study has two main goals: first to develop a conceptual, "hydroclimate period" framework to classify hydrologic function of a glacierized watershed and assess the dominant source waters during hydroclimatic periods. Second, we aim to quantify solute fluxes and their evolution throughout the melt season using this hydroclimate period framework to demonstrate how variable they can be over a melt season. To do so, we focus on the 25 km^2 Wolverine Glacier watershed, which is 60% ice-covered and has land cover representative of the larger coastal southcentral Alaska ecosystem (O'Neel et al., 2019).

Hydrograph classification has been used extensively to determine characteristic responses to hydroclimatic forcing and to better determine the mechanisms behind complex hydrologic process and flow paths (Olden et al., 2012). Specifically, it has been applied to glacierized watersheds using a range of methods, at various spatial and temporal scales (Curran & Biles, 2021; Hannah et al., 2000; Sergeant et al., 2020; Swift et al., 2005). Similarly, concentration discharge relationships have been used to determine watershed hydrologic function and water sources (Evans & Davies, 1998; Godsey et al., 2009; Maher, 2011; McGlynn & McDonnell, 2003). We suggest that the combination of these two approaches can yield powerful information on the shifting dominant source waters throughout the melt season and provide a foundation for comparison across watersheds or seasons. Our work leverages 15-min interval records of streamflow, specific

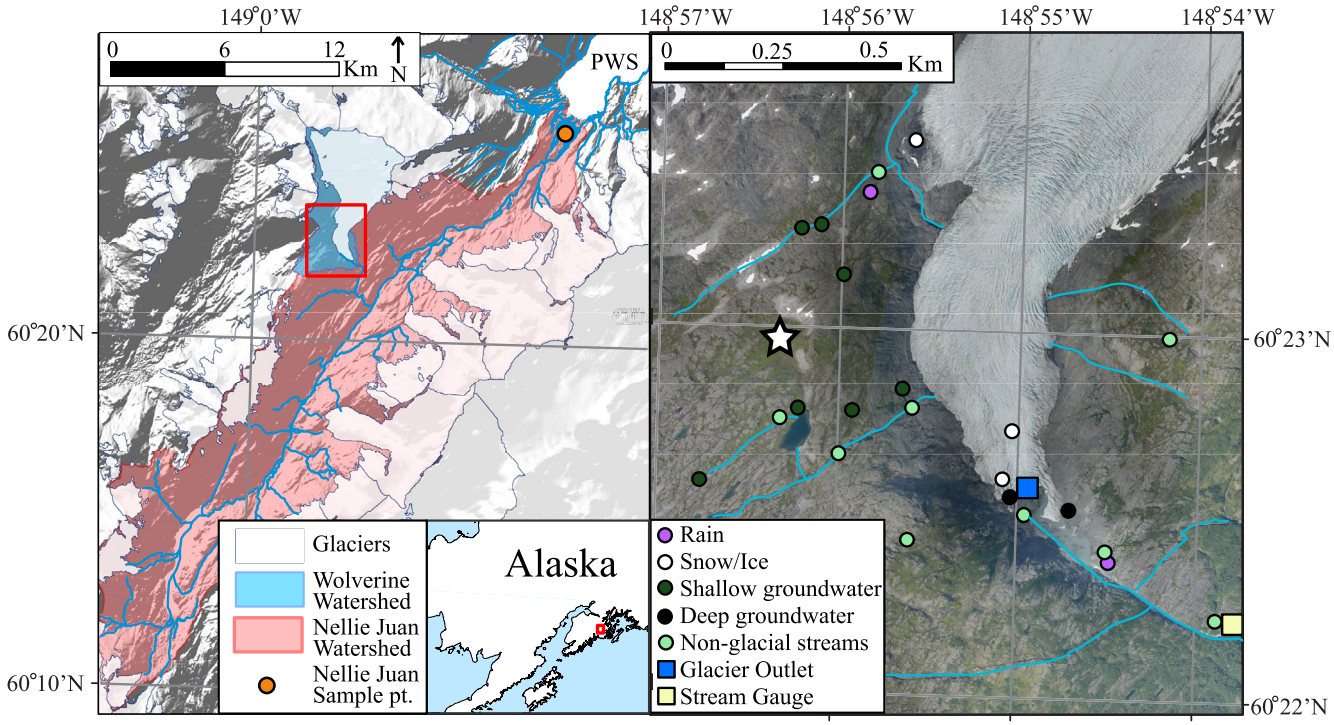

Figure 1. Site map of the Nellie Juan River watershed (left panel, red). The Nellie Juan River flows northeast to Prince William Sound (labeled PWS in upper right corner). The Wolverine Glacier watershed (blue in left panel) is a sub-watershed of the Nellie Juan River watershed. The red box in the left panel indicates the location of the subset sampling map at right. Colors correspond to sample type: rain, snow/ice, shallow groundwater, deep groundwater, nonglacial streams, glacier outlet, and Wolverine Creek streamgage. Locations sampled in both 2016 and 2017 are shown as squares. Locations only sampled in one season are circles. The meteorological station location is indicated by a white star in the inset map. The Nellie Juan River sampling site is shown as an orange point in the left panel.

conductance, and precipitation to characterize water and solute fluxes. We use concentration-discharge relationships and well-established typical alpine glacier hydrologic response patterns (Cuffey & Paterson, 2010; Fountain & Tangborn, 1985) to classify the runoff characteristics of a glacierized watershed into hydroclimatic periods and to assess the predictive capabilities of these data collected over two summers. We calculate export of calcium, the dominant ion in riverine export and a critical element in marine environments (Evans et al., 2014; Zhu & Macdougall, 1998), for each hydroclimatic period as a baseline for evaluating changes under future climate regimes.

2. Methods

2.1. Site Description

Wolverine Creek drains a 24.6 km^2, ~60% glacierized watershed (as delineated at the streamgage as the watershed outlet; Figure 1) located in the Kenai Mountains of southcentral Alaska (O'Neel et al., 2019). The region is dominated by accretionary terrains from the Valdez Group, which formed during the upper cretaceous and is composed of metasedimentary rocks, primarily graywacke, siltstone, and shale. The Wolverine basin falls in the zone of "undivided metasedimentary rocks," which is primarily composed of turbidites and includes uncommon but widely distributed conglomerate sandstones that may contain limestone (Wilson et al., 2008). The regional climate is maritime. At 990 m elevation (Figure 1, the location of the meteorological station), long-term annual-average temperature is −0.2°C and average precipitation rates exceed 3 m/year. A previous study found a significant (alpha = 0.1) warming trend of 0.02°C/year from the period of 1964 to present (O'Neel et al., 2019). In the upper watershed, where the weather station is located, at least 60%–70% of precipitation falls as snow. Most snow in the accumulation zone of the glacier becomes incorporated into the glacier through firnification. Snow melts seasonally both on- and off-glacier. Ice in

the ablation zone of the glacier also melts seasonally. The glacier-wide average ablation rate was −3.9 and −2.7 m water equivalent for the 2016 and 2017 summers, respectively (O'Neel et al., 2019).

Wolverine Glacier ranges over 1,000 m in elevation, with its uppermost elevation at 1,680 m (Van Beusekom et al., 2010). Landcover in the ice-free portions of the watershed varies primarily with elevation. The highest elevations are barren rock with limited or no soil and vegetation. The majority of the nonglacier watershed area is characterized by alpine tundra with sparse patches of willow, alder, dwarf spruce, and krummholz hemlock punctuated by bedrock outcrops and small ponds. Alder, willow, and cottonwood forests characterize the lowest elevations of the watershed. Evapotranspiration is not well constrained in this region but is likely low due to high humidity, low mean annual temperature, low biomass, and high proportion of bare ground in the watershed (O'Neel et al., 2019). Limited observations suggest that the tundra soils classify as Cryod-Cryorthent type or similar. These shallow (20–60 cm) soils are typically well-drained, acidic, and contain a high proportion of rock fragments (Patten, 2000).

The alpine tundra is drained by small streams, which in some cases flow into and under the glacier where they are incorporated in the subglacial flow. The glacier itself has a network of supra-glacial meltwater channels draining through moulins and crevasses to the base of the glacier feeding a subglacial drainage network, which exits the glacier terminus as one channel (Figure 1). The USGS installed the Wolverine Creek streamgage approximately 100 m from the glacier outlet in 1967 (Meier et al., 1971). Today, the glacier terminus is approximately 1.5 km upstream of the streamgage. Between the glacier outlet and the streamgage, ∼10 first order tributaries draining the surrounding tundra flow into Wolverine Creek, estimated to potentially increase discharge at peak snowmelt by up to 10%. Generally stream discharge is dilute, with maximum electrical conductivity (EC) less than 200 $\mu S\ cm^{-1}$.

Wolverine Creek flows for another ∼1 km below the streamgage before joining the Nellie Juan River, which in turn flows to Prince William Sound. The Nellie Juan River watershed is made up of many small watersheds similar to the Wolverine Glacier watershed in scale and landcover, which all flow to the large river system at the valley bottom (Figure 1). Glaciers cover approximately 40% of the 450 km^2 Nellie Juan River watershed. The USGS operated a streamgage on the Nellie Juan River from 1961 to 1965 and during that time, melt-season discharge averaged roughly 24 $m^3\ s^{-1}$. The lower elevations of the watershed support a coastal temperate rainforest ecosystem of hemlock, spruce, and cottonwood with an understory of alder and willow. At its delta, Nellie Juan River is a braided river system with a primary channel that empties into the Prince William Sound. Prince William Sound is a productive, inland marine environment with limited circulation with the Pacific Ocean. The large contribution of calcium carbonate from glacierized watersheds and limited oceanic circulation means that the Prince William Sound is particularly at risk to acidification with climate change (Evans et al., 2014).

2.2. Field Data and Sample Processing

Siting for the Wolverine Creek streamgage (USGS Streamgage 15236900, Wolverine C nr Lawing AK) consists of a well-defined bedrock channel. Although the record contains multiple data gaps, it has operated continuously through the melt season since 2001. Data are only available when the stream is not frozen, typically early May to early November. In the spring of 2016, water quality instrumentation measuring temperature, specific conductance, dissolved oxygen, pH, and turbidity was added to the streamgage.

In addition to the streamgage, the USGS also installed a weather station measuring temperature and precipitation in 1967. The station is located on the glacier margin at an elevation of 990 m, which is below the glacier's equilibrium line. This station was updated to measure wind in 1995, and with a weighing-type precipitation gage in 2012. Data have been quality-checked and averaged to the daily values used here (methods described in Baker et al., 2019).

The watershed can only be accessed via helicopter so we collected water samples in 3–7 days campaigns throughout the 2016 and 2017 melt seasons (April to October), targeting collection around independent water sources primarily classified by landcover or stream type (tundra, glacier, groundwater, mixed; Figure 1; Koch et al., 2021). In 2016, we made six trips and sampled the watershed in as many streams and landcover types as possible to characterize the site, then in 2017 we made five shorter trips and targeted sampling at the watershed-representative sites (Figure 1). We sampled at the streamgage and the outlet of the Nellie

Juan River in both years. We could only perform limited sampling at the streamgage and Nellie Juan River outlet for logistical reasons, limiting the size of the data set.

Exact sampling methods varied slightly by season. At each site, we rinsed a collection syringe or bottle three times with sample water prior to filtering. Water samples were collected using a 60 ml syringe placed directly into the water, or HDPE bottle in the case of low sample volumes or flows. Deep groundwater collection was made from seeps emanating from cracks in the exposed bedrock. We walked up slope to ensure that the seep was not being immediately recharged from a pool. Shallow groundwater was collected from seeps/return flow at breaks in slope of the upland hillslopes. Shallow and deep groundwater samples were collected from various elevations and landforms, and we confirmed our field inferences of shallow versus deep groundwater sources with a handheld EC meter in the field. Snow samples were collected in sterile Whirl pack bags, and snow was allowed to slowly melt in a cooler. Rain samples were collected from a triple deionized (DI) water rinsed plastic collection pan placed on the land surface during rainstorms that occurred while we were deployed to the field.

In 2016, samples were primarily filtered with a 0.45 μm Millipore filter, though some samples with very high glacial flour content were filtered with a pre-ashed GF/C filter. In 2017, all samples were field filtered with a 0.45 μm Millipore filter, which had been pre-rinsed with at least 200 ml of DI water. Sample bottles were all triple rinsed with filtered sample water prior to filling. No refrigeration is available in the remote field site, so samples were stored as cold as was possible in the field (in a snowbank, cooler, or sealed and submerged in a stream), and were immediately refrigerated or frozen upon returning to the lab.

Water was analyzed for water isotopes ($\delta^{18}O$ and $\delta^{2}H$) with a Piccaro cavity ring down spectrometer at the Klein lab at the University of Alaska, Anchorage (accuracy $<\pm 0.2‰$ for $\delta^{18}O$ and $<\pm 2‰$ for $\delta^{2}H$). Calcium concentration of 2016 samples was analyzed by inductively coupled plasma mass spectroscopy (Agilent ICP-MS, Applied Science Engineering and Technology Lab at the University of Alaska, Anchorage, minimum accuracy ± 0.4 mg l^{-1}). Calcium concentration of 2017 samples was analyzed by ion chromatography (Dionex IC, USGS labs in Boulder, CO, accuracy ± 0.1 mg l^{-1}).

We measured water quality parameters of each sampling location during sample collection with a multiprobe placed directly in the stream. In 2016 pH, temperature, electrical conductivity (EC), and total dissolved solids were measured with a Hanna Combo multiprobe (EC accuracy ±2%). In 2017, pH, temperature, and electrical conductivity were measured with a YSI 6920 V2-2 Multi-Parameter sonde (EC accuracy ±0.5%). Water quality probes were calibrated each morning prior to sampling.

2.3. Hydroclimatic Periods

Hydroclimatic periods were defined using a mixed qualitative and quantitative approach. We used initial observations, supported by previous glacio-hydrological research, to hypothesize that there are four distinctly different hydroclimatic periods. We examined the behavior of the relationship between electrical conductivity (EC) and discharge (Q) measured at the watershed outlet (Wolverine streamgage), supported by precipitation timeseries from the weather station located within the watershed, to define hydroclimatic periods (Figure 1).

We hypothesized four periods as follows: Winter and early spring flows are sustained by groundwater and slow subglacial/englacial drainage (Liljedahl et al., 2017; Malard et al., 1999) therefore the first period (P1) should have low Q and relatively high EC. In early spring, air temperatures and solar radiation increase resulting in snow melt reaching the glacier bed. The subglacial drainage network of most temperate glaciers transitions from a linked cavity system in winter to a tunnel system with low-pressure and high efficiency in summer, allowing faster meltwater drainage (Kamb et al., 1985; Werder et al., 2013). During this time, we hypothesize that there is a second period (P2) of transition that flushes water overwintered in the subglacial drainage network. This should be reflected as pulses of high EC in the record. In the next period (P3), seasonal snowpack melts both on- and off-glacier, causing streamflow to increase and diluting nutrient and solute concentrations (Fountain & Tangborn, 1985; Horton et al., 2006). Snowmelt should be a strong signal in the Wolverine watershed and we expect increasing Q and decreasing EC in P3. During this time, strong daily increases in temperature and radiation result in daily snow and ice melt pulses that are commonly reflected in Q and EC records (Nanni et al., 2019; Singley et al., 2017; Swift et al., 2005). In coastal Alaska (and other

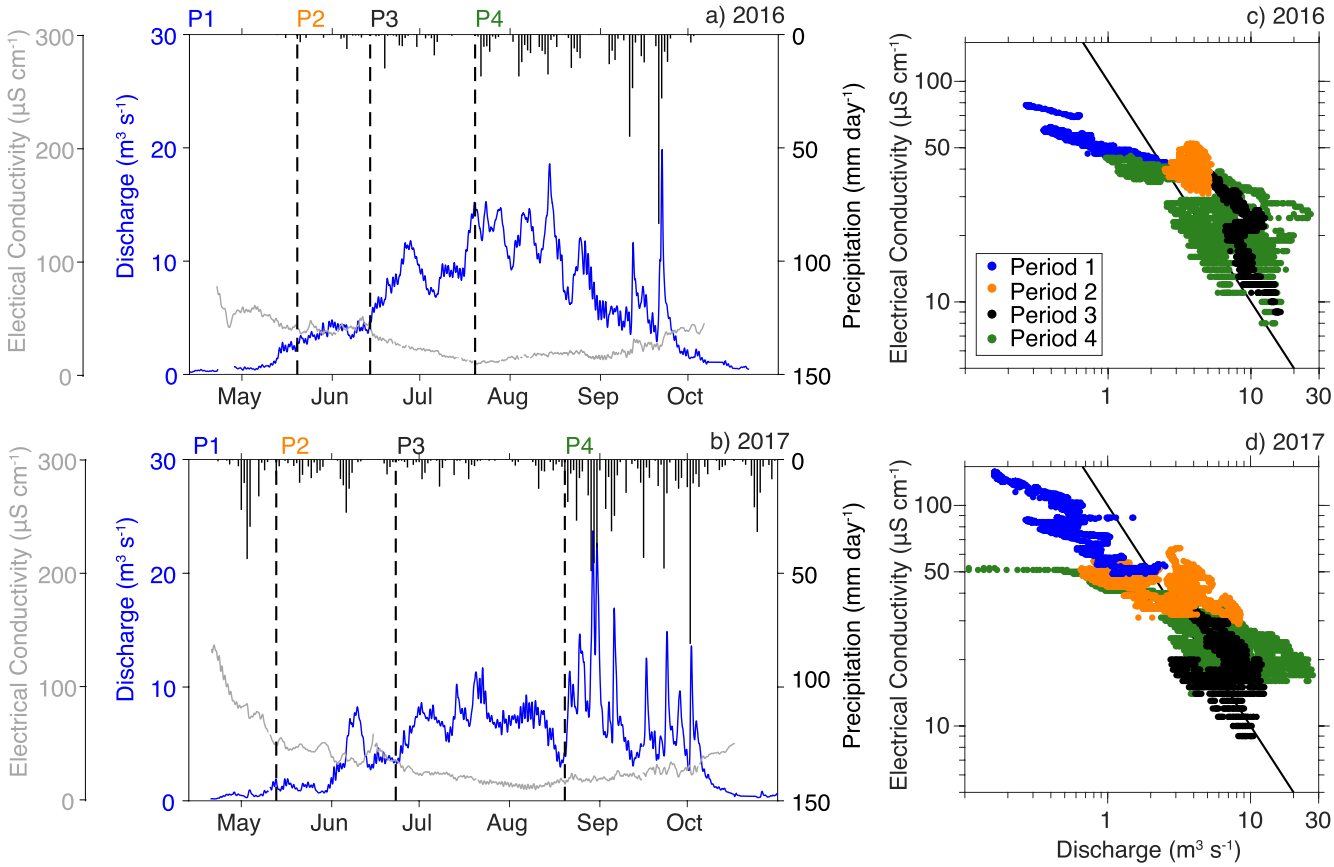

Figure 2. Records of discharge (blue), electrical conductivity (gray) from the Wolverine Creek streamgage and precipitation (black) from the 990 m meteorological station (Figure 1) in (a) 2016 and (b) 2017. Vertical dashed black lines divide each season into four hydroclimatic periods indicated by roman numerals: initial snowmelt, connection of the subglacial drainage network, main snowmelt, and rainy season. The relationship between discharge (Q) and electrical conductivity (EC) records at the Wolverine Creek streamgage are shown for (c) 2016 and (d) 2017. The record is divided into four hydroclimatic periods by color, matching the roman numerals in panels (a), (b).

coastal glacierized regions), a late-season rainy period characterized by an event-response based hydrograph occurs regularly as storms increase in frequency (Curran & Biles, 2021; Déry et al., 2009). We expect that a fourth period will be characterized by Q and EC responding to rain events with periodic increases.

We used an iterative process to partition records, focusing specifically on the EC-Q relationship with decisions on partitioning supported by precipitation timeseries. First, we visually examined EC and Q timeseries to determine broad transitions from one period to the next: for example, a switch from a long-term increasing trend (days to weeks) to a long-term decreasing trend (Figure 2). Then, we visually examined week-long windows centered around first order transitions in detail to define the exact timing of transition from one period to the next, for example, the onset of rainfall or a melt event. Additionally, we fit a power law function through the points in each period, a commonly used method to examine watershed behavior and solute release (e.g., Godsey et al., 2009). We combined both years in order to assess broad controls on solute export and to compare the relationship between EC and Q for each period (Ibarra et al., 2017). This fitting was done iteratively and aided in determining the appropriate number of periods and transition points between periods. For example, if the power-law fit for each proposed period was substantially different, we had confidence that the division was appropriate. If the power law fits were similar, the transition points were abandoned and new ones were tested.

The four periods were determined by abrupt shifts in behavior of the EC-Q relationship, implying a transition from one period to the next. The transition time between P1 and P2 was determined as a switch from a continuously negative EC-Q correlation to no distinct pattern (Figures 2c and 2d). The transition from P2 to P3 was identified as a switch in the EC-Q relationship to a more negative exponent in the power law

Table 1
EC and $\delta^{18}O$ of the Major Source Waters of the Wolverine Glacier Watershed: Bold Number is an Average of All Samples for a Given Source Across Both the 2016 and 2017 Seasons With the SD in Parenthesis and the Number of Samples Used for the Estimate

	EC (µs/cm)	$\delta^{18}O$ (00/0)
Rain	10 (6) $n = 4$	−11.3 (4.2) $n = 5$
Snow/ice	11 (16) $n = 14$	−17.4 (3.3) $n = 41$
Shallow GW	83 (33) $n = 11$	−15.3 (0.9) $n = 14$
Deep GW	159 (65) $n = 10$	−13.2 (1.4) $n = 7$

relationship coincident with a sharp increase in Q (Figure 2). The onset of diel EC and Q pulses also distinguishes the start of P3, The transition between P3 and P4 is the most subjective and based on three factors: an increase in Q from precipitation, the timing and magnitude of precipitation events, and the switch from a long-term decreasing EC trend in P3 to a long-term increasing trend in P4. These three factors never occurred simultaneously, and we used an average timing of these factors to establish the transition from P3 to P4 supported by power law fits.

2.4. Mixing Model for Source Water Attribution

We sampled at two main stream types within the Wolverine Glacier watershed: nonglacial streams and the glacier outlet stream located at the glacier terminus (Figure 1). We applied a three-component end member mixing model to determine the relative contributions of source waters to each stream type (nonglacial and glacier outlet) in each hydroclimatic period (Burns et al., 2001; Liu et al., 2004). Tracers included $\delta^{18}O$ and EC. EC was chosen as a tracer given (a) that it clearly separated meteoric and ground water and (b) that the water sources were dilute, which meant that specific solutes (e.g., chloride) were often below detection. We believe that EC is an appropriate tracer given the short travel times and dilute and turbid water that limits reactivity of the major ions that contribute to the EC signature. The mixing model was formulated as:

$$1 = f_{\text{rain}} + f_{\text{snow/ice}} + f_{\text{gw}} \tag{1}$$

$$C_{\text{stream}} = C_{\text{rain}} f_{\text{rain}} + C_{\text{snow/ice}} f_{\text{snow/ice}} + C_{\text{gw}} f_{\text{gw}} \tag{2}$$

where C is the EC or the $\delta^{18}O$ signature and f is the fraction of each of the source waters. For the C_{stream} value, we calculated an average of all samples collected in the nonglacial streams and an average of all glacier outflow samples for each period, in order to make broad comparisons of the relative influence of glacier and nonglacier dominated parts of the watershed. We also examined water chemistry at the scale of the Wolverine Creek streamgage and Nellie Juan River watershed. However, due to access challenges constraining the number of samples we could collect, we limited our analysis to more qualitative inferences within the mixing space, rather than apply this mixing model approach.

We determined four main water sources within the Wolverine Glacier watershed: rain, ice/snow, shallow groundwater, and deep groundwater, each with distinct combination of EC and $\delta^{18}O$ signatures (Table 1), which was determined using a multiple comparison method of a one-way analysis of variance (ANOVA) to test for differences among end members (Figure S1 in Supporting Information S1). Rain, ice/snow, and deep groundwater were selected for the mixing analysis because they fully constrained the samples within the mixing space. We did not have a suitable third tracer in our data set to include shallow groundwater. Rain samples may have been affected by evaporation prior to collection (Figure S2 in Supporting Information S1). However, we choose not to correct the samples due to lack of data and the fact that the uncorrected rain samples appear to frame the nonglacial and glacier outlet samples quite well.

In order to assess the impacts of limited sample sizes and the accuracy of the end-member calculations, end members were selected from a random uniform distribution in the range between the mean and 1 SD of the end-member samples. The randomly chosen end member was applied to a mixing calculation (Equation 2) for all four periods and only retained if positive fractions were calculated (i.e., negative, nonmeaningful results were thrown out). This approach ensures that no mixing fraction is negative and that all chosen end members bound the data set. This process was repeated 10,000 times, typically generating nonnegative results in around 24% of runs. Negative fractions were solely related to the condition when the randomly chosen snow/ice endmember had less negative $\delta^{18}O$, or greater EC than the stream water.

2.5. Flux Estimates

We derived calcium (Ca^{2+}) flux estimates from the empirical relationship between Ca^{2+} concentration and EC. We did not have full solute chemistry for these samples, so we were not able to calculate a total solute

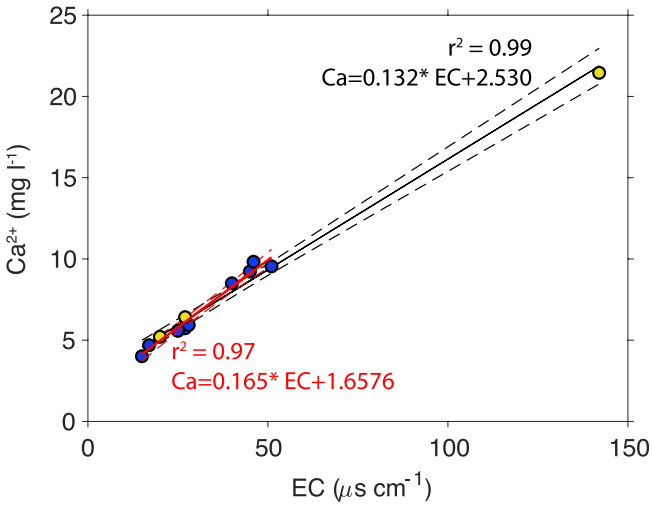

Figure 3. Linear regressions between electrical conductivity and Ca^{2+} concentration using grab samples collected in the 2017 season at the streamgage (yellow points) and glacier outlet stream (blue points) in the Wolverine Glacier watershed. One regression was calculated with all the data (black) and the other was calculated without the outlier sample from the streamgage (red).

flux. However, Ca^{2+} is the dominant cation and we believe that it is a suitable proxy for total solute flux. We built the regression using contemporaneous EC measured at the streamgage and Ca^{2+} grab samples collected both at the streamgage and glacier outlet. We found a robust linear relationship between EC measured at the glacier outlet at the time of grab sample collection and EC recorded simultaneously at the streamgage: $R^2 = 0.93$, $p << 0.05$, indicating minor changes in stream chemistry over the intervening reach (Figure 3). To estimate a Ca^{2+} concentration timeseries for both the 2016 and 2017 seasons, we used the linear relationship between EC and Ca^{2+} ($R^2 = 0.99$, $p << 0.05$):

$$Ca_i = 0.132 * \mathrm{EC}_i + 2.530 \quad (3)$$

where EC_i are the 15-min observations and Ca_i are the sample Ca^{2+} concentrations. Calcium flux at the streamgage was determined by multiplying the concentration timeseries with the discharge timeseries. Total exports per hydroclimatic period were calculated by integrating over each period:

$$Ca_{P_j} = \int_{P_j} Ca^{2+} * Q\, dt \quad (4)$$

where P_j is one of four hydroclimatic periods. Results are presented in specific units of meq m^{-2} $year^{-1}$ by scaling by the watershed area to easily compare across other weathering studies. The points used to develop the EC-Ca^{2+} relationship had one sample with very high EC and Ca^{2+} collected at the streamgage. We did a second regression and set of flux calculations excluding that point to determine the degree that outliers affect Ca^{2+} flux estimates. Calcium and other major ions are expected to behave conservatively over the short travel distances (on the order of kilometers) and times (on the order of hours from the glacier to the stream gage), especially given that the stream is dilute, cold, and turbid.

3. Results

3.1. Hydroclimatic Periods

The timeseries of electrical conductivity, discharge, and precipitation show clear seasonality for both 2016 and 2017 (Figures 2a and 2b). Discharge (Q) increases in steps from the beginning of the record to a peak in mid-summer. Q then follows an overall declining trend with rain event-response dynamics. In contrast to Q, EC decreases from the beginning of the melt season through late July or early August, when it begins to increase. Both Q and EC undergo shifts in short-term (less than weekly) variability, with periods of clear diel variations, and other periods where the diel signals are less pronounced or obscured by longer timescale variability.

We observed some early season precipitation (rain and snow) events, particularly in 2017, but the majority of precipitation was in the form of large late season rain events. The onset of the rainy season occurred earlier in 2016; however, in total, more rain fell in 2017. These patterns, and particularly the distinct relationships between EC and Q (Figures 2c and 2d), are distinct among the hydroclimatic periods.

The onset of snowmelt runoff characterizes hydroclimatic period one (P1). During both years, a significant reduction of EC (dilution) with minimal increase in Q characterizes P1 as shown in Figure 2. This drop in EC is particularly apparent in 2017 (Figures 2b and 2d). Despite a precipitation event of mixed rain and snow, Q remained steady through P1 in 2017. This behavior was consistent across 2016 and 2017, even with different climatic forcing. The fit of the power law relationship is good for P1 ($R^2 = 0.7$) and the exponent is the most negative for this period, meaning it is the closest to a pure dilution signal relative to the other three periods (Table 2).

The exponent of the power-law fit between EC and Q in P2 is −0.14, closest to 0 relative to the other three periods, suggesting near chemostasis and a functional shift between P1 and P2 (Table 2). Although highly

Table 2
Power Law Fit of Electrical Conductivity (EC) and Discharge (Q) Measured at the Streamgage Divided by Hydroclimatic Period

Period	*a*	*b*	R2
P1	54	−0.48	0.70
P2	48	−0.14	0.43
P3	39	−0.32	0.08
P4	44	−0.36	0.70

Note. Power law fits follow the equation: $EC = aQb$.

variable, EC lacks obvious periodicity, for example, diel, in hydroclimatic period 2 (P2, Figure 2). Discharge does exhibit diel pulses and continues on an upward trend. A precipitation event occurred in 2017, complicating the discharge response by superimposing high-flux storm response over a slower seasonal Q increase (Figures 2c and 2d, orange points). Despite this, we found similar overall behavior in P2 across 2016 and 2017.

We observed that EC regains diel periodicity in P3 and continued to decline, although more gradually than in P1 (Figure 2). Discharge increased with apparent high baseflow and also exhibited diel behavior. The EC-Q relationship zig-zagged toward lower Q and EC with greater variability in EC than Q (Figures 2c and 2d, black points).

The start of P4 coincided with a substantial increase in Q and a flashy response to rain events (Figure 2). The defining characteristic in the relationship between EC and Q for this period was that it was largely chemostatic: EC remained near the same level despite large increases in Q. Dilution was present but minor (Figures 2c and 2d, green points). The fit of the power law relationship improved substantially between P3 and P4 (R^2 shifts from 0.08 to 0.70; Table 2). The exponent of the P4 relationship was −0.36, indicating some dilution, but less than P1 (Table 2). Additionally, baseline EC gradually increased.

3.2. Source Water Chemical Signatures

When examined through the lens of the hydroclimatic periods, there are distinct differences in source water contributions and resulting water chemistry through the flow season. The relationship between EC and $\delta^{18}O$ illustrate distinct chemistries for each water source (Table 1). Our data do not support differences between snow melt and ice melt, and we characterize these meltwater sources together. Meltwater exhibits the most negative $\delta^{18}O$ among the source types. Despite limited rain samples, $\delta^{18}O$ in rain is more positive than in snow/ice sources. Both precipitation source types, rain and snow, exhibit high variability in $\delta^{18}O$ in accord with variable storm sources and histories (Dansgaard, 1964; Gat & Dansgaard, 1972; Lachniet et al., 2016; Stewart, 1975). Both rain and snow/ice sources have relatively low EC (means of 10.2 and 13.1 $\mu S\ cm^{-1}$, respectively), and stream waters were quite dilute, never exceeding 200 $\mu S\ cm^{-1}$ (Figure 3). Calcium was the dominant ion in all samples, on the order of 25% of the solute load, based on limited full suite chemical data from 2016 to 2017 (Koch et al., 2021) and confirmed with more robust sampling in 2019 and 2020. Calcium concentrations averaged $6.5 \pm 4.5\ mg\ L^{-1}$ ($n = 116$), with the highest concentrations in groundwater seeps ($15 \pm 3\ mg\ L^{-1}$, $n = 7$), all of which are well below expected saturation in these cold, circumneutral waters.

Samples from numerous groundwater seeps suggest that two major groundwater source chemistries exist in the watershed. What we define as shallow groundwater has depleted $\delta^{18}O$ similar to snow and ice melt and lower EC relative to deep groundwater. Water collected at lower elevation in the watershed from bedrock outcrop seeps is characterized by less depleted $\delta^{18}O$ and much higher EC relative to the shallow groundwater. Source water chemistry had little temporal variability.

3.3. Seasonal Trends in Stream Chemistry

The distribution of nonglacial streams and glacier outlet stream samples both fall within the bounds of the respective source waters (Figure 4). Source waters and mixtures exhibit clear separation in EC—$\delta^{18}O$ space. In P1, the nonglacial streams are closer to the snow and ice signal than the glacier outlet stream samples, which trend slightly toward groundwater (Figure 4a). By P2 the nonglacial streams have increasing $\delta^{18}O$ signatures but maintain low EC, which persists through P3. By P4 in 2016, the nonglacial streams plot on two distinct lines between the rain source and shallow groundwater, and between rain and deep groundwater (Figure 4d, filled green circles). This trend was not observed in 2017.

The glacier outlet stream samples start with relatively high EC in P1, decreasing slightly in P2. During the main snow and ice melt, characteristic of P3, the glacier outlet stream samples have little variability and are very close to the snow and ice source water signature. However, by the P4 rainy season, the glacier

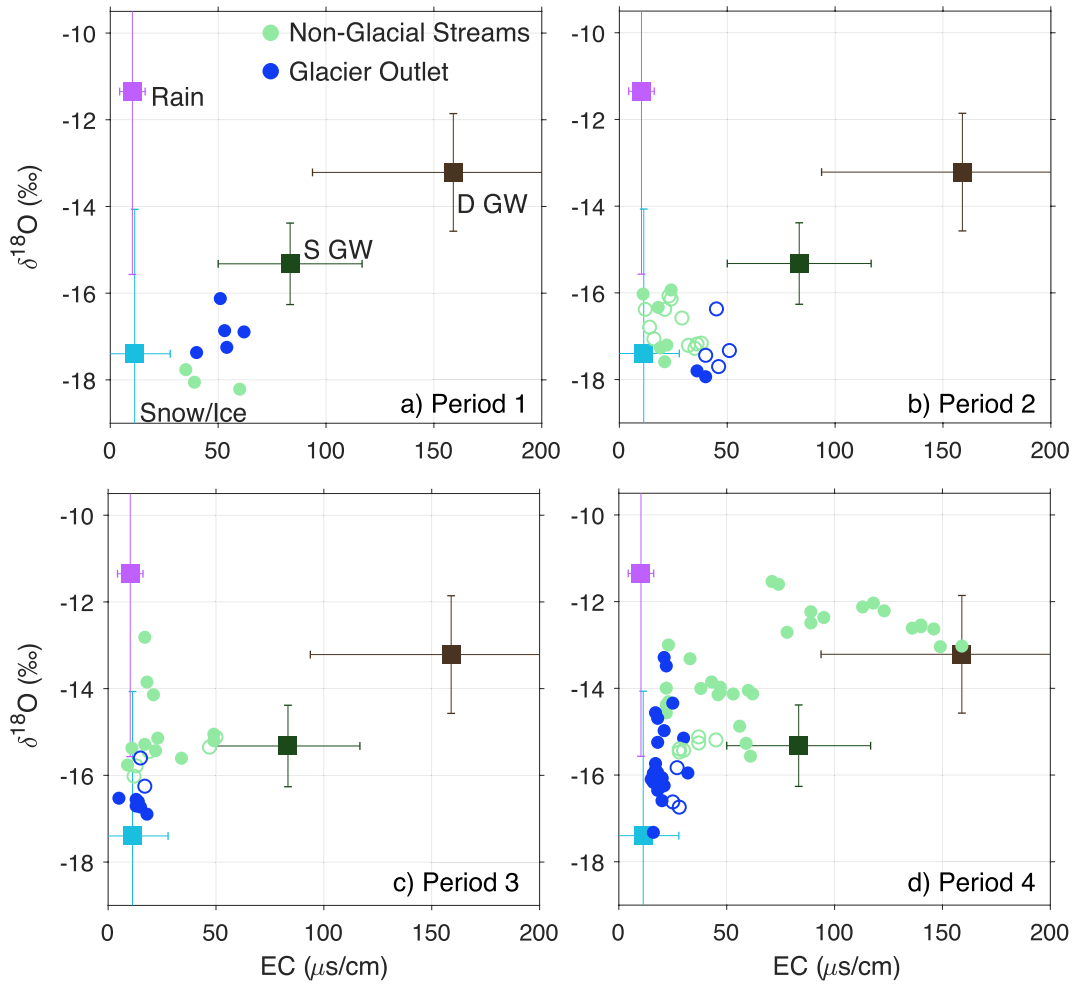

Figure 4. The relationship between electrical conductivity (EC) and $\delta^{18}O$ for all nonglacially fed streams and glacier outlet water samples taken in the 2016 (filled circles) and 2017 (open circles) divided by hydroclimatic period. The mean value of major source waters (filled squares) with SE (error bars) are shown and constant across all four hydroclimatic periods. End members are labeled in a) rain, snow/ice, shallow groundwater (S GW), and deep groundwater (D GW).

outlet stream has consistently low EC but a wide range of $\delta^{18}O$ approaching the signature of the rain source (Figure 4d).

The results of the mixing model quantify the relative contributions from sources to both nonglacial and glacier outlet samples for each period in 2016 and 2017. We do not have samples from P1 in 2017, but in 2016, P1 suggests a relatively high groundwater contribution for both nonglacial streams (21 ± 5% in 2016) and the glacier outlet stream (29 ± 7% in 2016) (Figures 5a and 5b). The proportion of groundwater decreases as the rain and snow/ice fractions increase. In both years, the glacier outlet streams have a much lower groundwater fraction in P3 and P4 relative to the earlier periods (Figures 5a and 5c). The snow/ice fraction is relatively stable across periods for the glacier outlet stream but decreases over time for the nonglacial streams. The groundwater fraction is depressed in the middle two periods for nonglacial streams (5%–11%) and is higher in P1 and P4 in 2016 (21 ± 5% and 41 ± 9%) and slightly higher in P4 in 2017 (16% ± 6%, Figure 5).

3.4. Spatial Scaling of Mixtures From Headwaters to Ocean

At larger spatial scales, samples fell within the source water end members, but seasonal trends varied. The Wolverine Creek streamgage has a signature very similar to the glacier outlet despite the fact that it

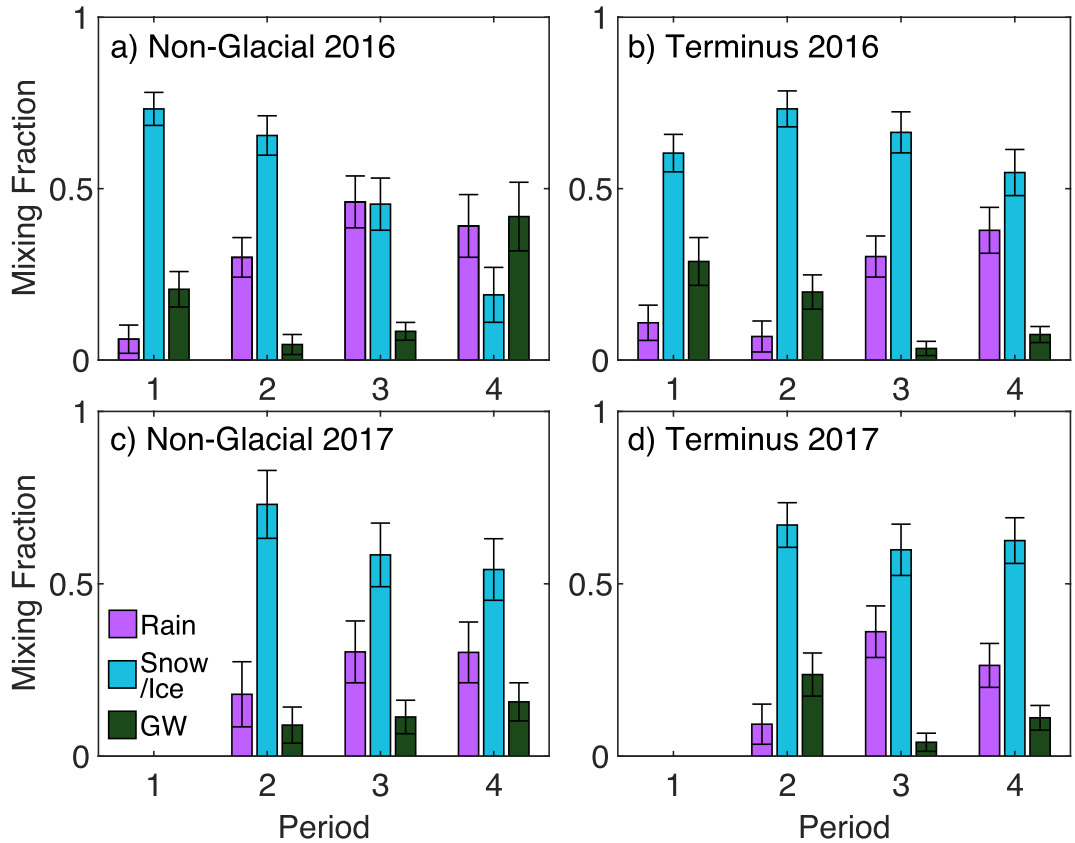

Figure 5. Fraction of source waters as determined by a three-component mixing model for (a), (c) nonglacial and (b), (d) glacier outlet samples collected in (a), (b) 2016 and (c), (d) 2017. The deep groundwater signature was used as the groundwater end member for this analysis. We were not able to collect samples from period 1 in 2017 and therefore have missing data for that time.

incorporates slightly more nonglacial area (Figures 1 and 6). In P1, the streamgage is chemically similar to the nonglacial streams. Through the rest of the season, the streamgage samples are more similar to the EC and $\delta^{18}O$ signature of the glacier outlet (Figure 6). The EC and $\delta^{18}O$ signatures of the Nellie Juan River are remarkably stable across all four hydroclimatic periods and similar to the nonglacial streams in the Wolverine Glacier watershed only during the major snow and ice melt period (P3). As the nonglacial streams move toward a groundwater EC and $\delta^{18}O$ signature at the end of the season, the Nellie Juan River samples barely shift (P4, Figure 6d).

3.5. Calcium Flux at the Watershed Outlet

Calcium flux rates were highly variable across hydroclimatic periods (Figure 7, Table S1 in Supporting Information S1). P1 produces very little Ca^{2+} and makes up less than 4% of the total seasonal export. EC is high in P2 (Figure 2), but Q is very low, and the period is of short duration so fluxes and proportional contributions are lower than one might expect given the high EC (Table S1 in Supporting Information S1). The highest daily fluxes occur during peak snow and ice melt (P3). However, because the rainy season makes up a longer period of time, it contributes the highest percent of total solute flux. P2 has higher fluxes than P4 in 2016 but not in 2017. The regression excluding the high concentration streamgage sample has a higher slope and lower intercept than the regression with all the data (Figure 3). The resulting flux estimates present the same overall pattern across periods. Flux estimates made using the regression excluding the outlier are only 4%–7% different than those made including the outlier (using the kg/day value).

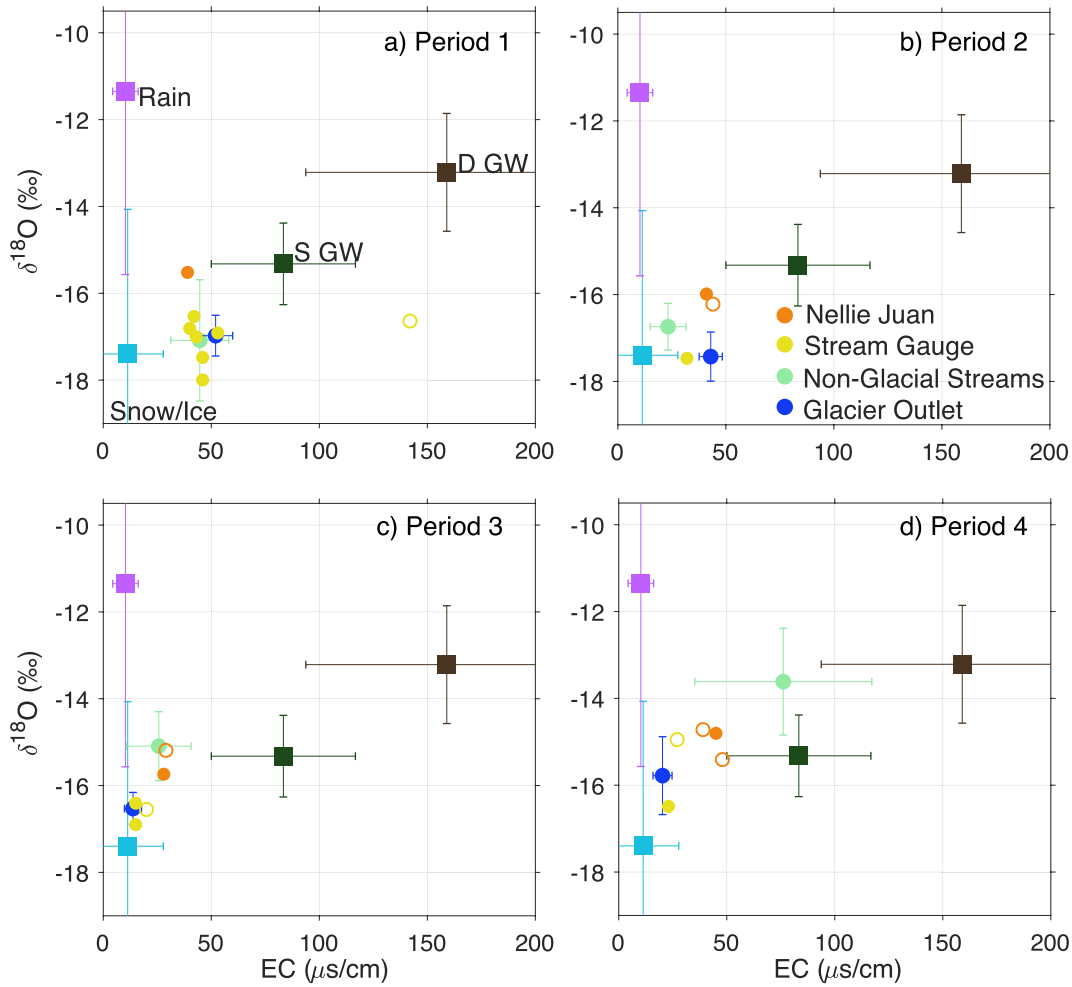

Figure 6. Electrical conductivity (EC) and $\delta^{18}O$ across scales: Wolverine Creek streamgage (yellow points) to the Nellie Juan River watershed outlet (orange points) for 2016 (filled circles) and 2017 (open circles). Nonglacial stream samples, glacier outlet stream samples (variable across periods), and the four source waters (constant across periods) are shown as an average with error bars representing SE.

4. Discussion

4.1. Classification of the Melt Season as an Analytical Framework

By combining classification of streamflow and EC-Q signatures with water sampling and source attribution, we derive a transferrable conceptual framework to partition glacierized catchment hydrographs and better estimate solute fluxes. Although concentration-discharge relationships have been employed in glacierized watersheds (Anderson et al., 1997, 2000; Axtmann & Stallard, 1995; Hodson, Porter, et al., 2002; Hudson, Tranter et al., 2002; Wadham et al., 1997; Yde et al., 2005), the scientific community has yet to fully characterize controls on solute fluxes from these environments (Anderson et al., 1997; Torres et al., 2017) or leverage solute-discharge relationships to gain process understanding and predictive capability. Our results suggest that this is due to high temporal and spatial variability in contributions from water sources across glacierized watersheds, each with unique solute concentrations (Figure 1). Moreover, field studies tend to be temporally limited, resulting in characterization of solute fluxes over a period that may not be representative of the entire melt season (Krawczyk et al., 2003). As a result, understanding and accounting for time-variable or complex concentration-discharge relationships (i.e., diluting, concentrating, and chemostatic) due to shifting sources, flow paths, and residence times may not be represented in estimates of solute flux.

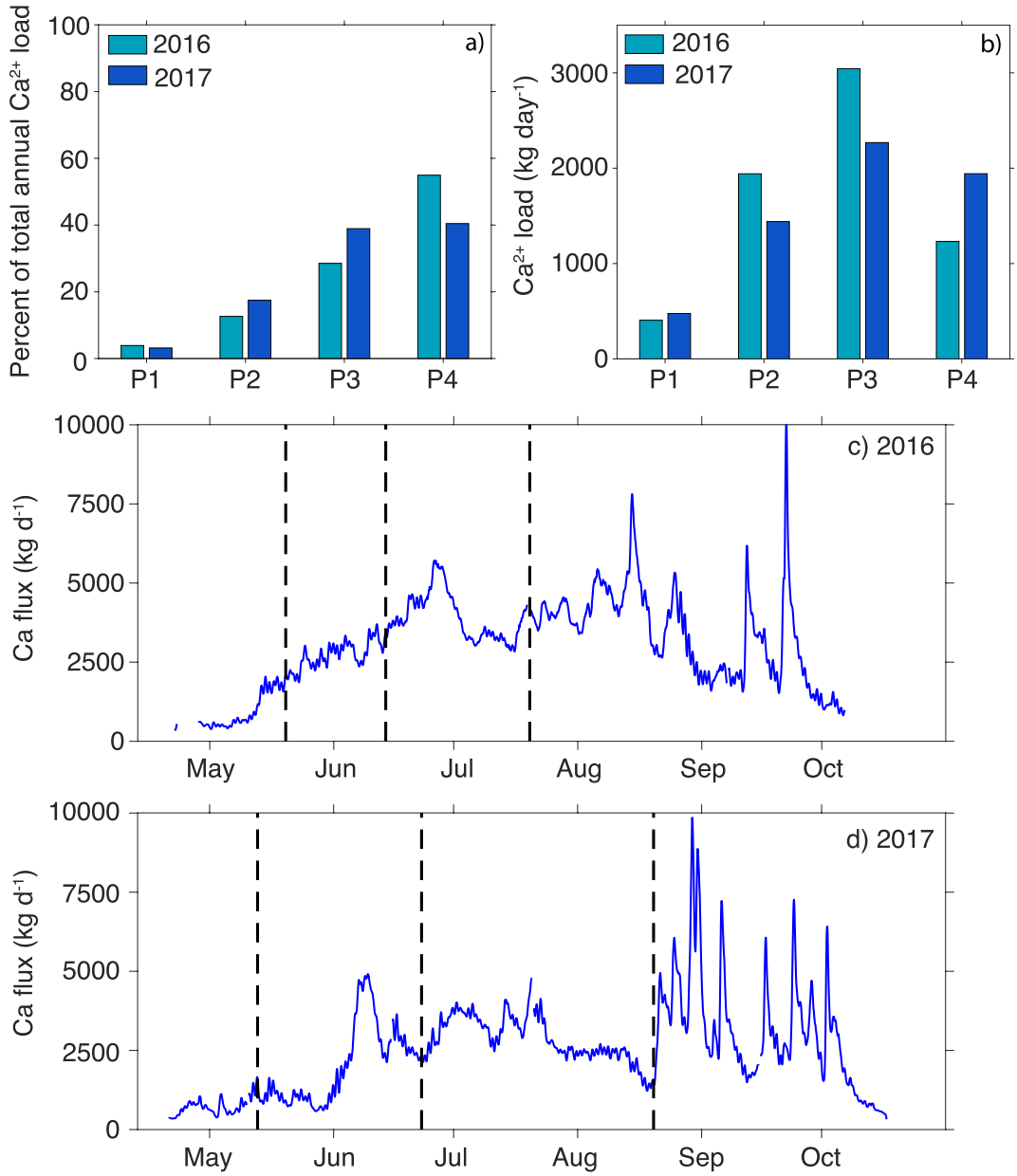

Figure 7. (a) percent of total annual Ca^{2+} flux divided by hydroclimatic periods for the 2016 and 2017 seasons. (b) Ca^{2+} flux by hydroclimatic period. Time series of calcium flux over the (c) 2016 and (d) 2017 flow seasons are also shown with vertical black dashed lines indicating divisions between the four hydroclimatic periods.

Solute flux is nearly always calculated as discharge multiplied by solute concentration integrated over some period of time. Whereas discharge is typically a continuous measurement, concentration is frequently estimated from discrete samples and regressions are employed to develop continuous solute concentration records through time over the hydrograph (e.g., Dolan et al., 1981; Likens et al., 1967; Ross et al., 2018). Weathering-derived solute fluxes in glacierized watersheds are frequently given with no indication of the method used or discussion of potential pitfalls of transferring a relationship across the entire melt season, between watersheds, or across scales (e.g., Dessert et al., 2003; Suchet & Probst, 1995; Torres et al., 2017) is an effective proxy for solute flux (Hodson, Porter, et al., 2002; Hudson, Tranter et al., 2002). We found that solute flux can be highly variable throughout the year (Figure 7). If we extrapolate measurements made in the early season of 2016 (P1), we calculate a Ca^{2+} flux of 406 meq m^{-2} $year^{-1}$. However, if we only use measurements made in peak melt of 2016 (P3), we calculate a Ca^{2+} flux of 3,044 meq m^{-2} $year^{-1}$,

approximately 7.5 times higher. Annual Ca^{2+} flux calculated using variable flux for the hydroperiods is 1,006 meq m^{-2} $year^{-1}$, assuming all solute export occurs during the period of record. We know that flow occurs most of the year so this is a low estimate, but we can say that annual flux as not as high as the P4 flux estimate. Furthermore, we expect that the exact composition of the exported solutes will also shift as different flow paths and water sources are activated (see Section 4.2). This suggests that it is not sufficient to collect samples in a limited time window and expect to get an accurate annual flux from glacierized watersheds without considering the hydrologic context of when the samples were collected. The advent of low-cost continuous water quality sensors provides a way to address these challenges (McKnight et al., 2015). Here, we demonstrate that EC can be collected through the entire melt season and provide an effective proxy for solute flux at high temporal resolution.

We defined four hydroclimatic periods that represent time-varying hydrologic process common to most glacierized catchments and therefore can be widely transferrable (e.g., Curran & Biles, 2021; Fountain & Tangborn, 1985, see Sections 2.3 and 4.2). Here the divisions between periods were manually determined, leveraging the stark differences between periods; however, a machine learning-based approach can be developed and is the subject of ongoing work. While the exact length and characteristics of each period is expected to vary from one water year or region to the next, this definition of hydroclimatic periods can be broadly used as a framework for parsing the flow season of glacierized watersheds over a range of climate regimes and/or fraction of glacier covered area. For example, while we found different transition times and durations of each period across 2 years, primarily as a result of precipitation forcing (Figure 2), broadly consistent hydrologic behavior allowed us to use the same hydroclimatic classification across two melt seasons with very different forcing. Furthermore, the shifting of the onset and duration of each of these periods over multiyear timescales can be a useful tool to understand how an individual glacier or watershed is responding to climate.

4.2. Relative Influence of Glacial and Nonglacial Water Sources Through the Melt Season

Snowmelt begins in early spring as daytime air temperatures exceed 0°C. In the Wolverine Glacier watershed, this initial melt period has greatest observed dilution of any period (Figure 2, Table 2) and a shift toward the snow and ice source water chemistry, particularly for the nonglacial streams (Figure 4a). Similarly, a large decrease in EC has also been observed in a polar/subpolar watershed in northeast Greenland, suggesting this behavior is not limited to mid-latitude systems (Rasch et al., 2000). There is some separation between the chemical signature of the glacier outlet stream and nonglacial streams at this time (P1, Figure 4a). Specifically, the glacier outlet has less depleted $\delta^{18}O$ than nonglacial streams. The glacier outlet stream is likely derived from winter storage in the subglacial drainage network or deeper groundwater, and is not yet receiving water from snowmelt in the surrounding watershed (Bhatia et al., 2011). Mixing model results indicate that the glacier outlet stream is, on average, 28% ± 7% groundwater in this period, the highest all season (Figure 5). In P1, the earliest snowmelt contributes to storage within the snowpack and subglacial drainage network, resulting in very long travel times for meltwater to reach the glacier outlet (Campbell et al., 2006; Hindshaw et al., 2011; Hodgkins, 2001; Singh et al., 2011; Zuecco et al., 2018). We found that P1 does not contribute much to the total annual inorganic solute flux from the Wolverine Glacier watershed (Figure 7, Table S1 in Supporting Information S1) due to the low flow, dilution from snowmelt, and brevity of the period. Although we do not rigorously report nutrient concentrations here, we suggest that the high EC and hypothesized contribution from groundwater we observe at the start of each season merits further study as it may be important to the riverine and marine ecosystems (Hood & Scott, 2008; Statham et al., 2008). The watershed and season-specific coupling of solute sources, climate, hydrologic flow path routing, and residence time drives differences in solute fluxes across glacierized watersheds and emphasizes the necessity of data collection during the early melt period.

The two melt seasons over which this study was conducted exhibit variability in both duration and amount of precipitation that fell in each period; for example, large spring rain events occurred in 2017 but not in 2016 (Figures 2a and 2b). Particularly, a spring storm on June 4–8, 2017 delivered 51 mm of rain. This resulted in a peak in Q followed by a 30 μS cm^{-1} EC increase (Figure 2b). This juxtaposition provides context and insight into potential future conditions. The more negative slope of the EC-Q relationship and earlier onset of P2 in 2017 conforms with the precipitation history (Figure 2). In a warmer future, we expect increased

precipitation as rain in the spring, which will hasten the onset of snowmelt and may shorten the tundra melt season—a shortened P1 and an earlier transition to P2 (Figure 2; Mcafee et al., 2014). Additionally, increased early season rain is likely to force earlier connection of the subglacial drainage network (e.g., Harper et al., 2002). However, there is added complexity because if melt begins earlier, the amount of radiative energy is lower, resulting in slower melt in an earlier spring scenario: an earlier onset of P1 rather than a shortened P1 (Musselman et al., 2017). The intersection of timing of precipitation and melt across the periods produces variable flux rates and proportional contributions to the total seasonal solute export (Figure 7; Fairchild et al., 1999; Rada & Schoof, 2018).

We observed large increases in EC (15–30 $\mu s\ cm^{-1}$) decoupled from Q during P2 in both 2016 and 2017, resulting in no clear EC-Q relationship (Figure 2, Table 2). These EC increases can come from two possible sources: connection and flushing of the subglacial drainage network (e.g., Fountain & Walder, 1998) or connection and flushing of nonglacial flow pathways (e.g., Evans et al., 2018; Spence & Woo, 2003). During this period, the nonglacial stream samples all have EC lower than glacier outlet stream samples (Figure 4b). Nonglacial areas appear to be dominated by highly dilute snowmelt water in shallow and overland flow paths (e.g., Carey et al., 2013; McGlynn et al., 1999). The relative contribution of groundwater to nonglacial streams is lowest in this period in both years (Figure 5). However, the EC values observed at the glacier outlet are of similar magnitude to the peak EC values observed at the streamgage, supporting the hypothesis that previously isolated or slow-draining parts of the subglacial system with high solute concentrations may be connected and flushed (Fountain & Walder, 1998; Nienow et al., 1998) and can influence the chemistry of the entire watershed (Figures 2c, 2d, and 6b). Solute flux was much higher in P2 associated with release of over-wintered subglacial water. However, due to the brevity of this period, it contributes little to total annual solute fluxes (Figure 7, Table S1 in Supporting Information S1). Water stored subglacially over long periods has unique solute chemistry due to long water-rock contact times and microbial activity (Tranter et al., 1997), and though this period might not contribute substantially to total solute flux, the unique biogeochemical composition (Hood et al., 2009) may make this pulse of water an important source of nutrients and solutes for downstream ecosystems (Carey, 2003; Koch et al., 2013; Raymond et al., 2007; Stubbins et al., 2012).

As the subglacial drainage network progressively transitions to an efficient drainage system, average stream water residence times decrease and water at the outlet resembles rain, meltwater, initiating P3 (Figures 2, 4c, 5, and 6c; Cuffey & Paterson, 2010; Hindshaw et al., 2011). The duration of P3 is a function of winter snow accumulation dictating available seasonal meltwater and the energy balance driving snowmelt (summer temperature and radiative forcing). The 2017 summer was cooler than 2016 resulting in a longer, more gradual snowmelt (P3, Figure 2). Seasonal snowmelt far outweighs annual glacier mass loss contributions to summer streamflow (O'Neel et al., 2014). Therefore, the highly probable scenario of warmer melt seasons following low snow accumulation (Littell et al., 2018) favors a future with rapid snowmelt and a shortened P3. Alternatively, a scenario where air temperatures remain slightly above freezing early in the season with very little available radiative energy will likely prolong P1 and P2. As tundra snow melts and seasonally frozen ground thaws, streams become increasingly groundwater dominated, with longer subsurface residence times and increased solute concentrations (Figure 5; Evans & Davies, 1998; Williams et al., 2009). As a result, the P3 EC decline slows and eventually reverses (Figure 2).

Solute fluxes are highest during P3 (Figure 7, Table S1 in Supporting Information S1). There are several possible drivers for high solute fluxes including high Q (Hood & Berner, 2009) and the deepening of soil flow pathways into mineral layers (Carey et al., 2013). Samples from nonglacial streams suggest that water flow to streams is likely still mainly restricted to overland flow and shallow soil (Figures 4c and 5). Even if water is being delivered as rain (indicated by less negative $\delta^{18}O$), little appears to move through deeper flow paths, as we generally do not observe increased EC (Figure 4c). However, we did collect several samples from nonglacial streams with higher EC ($>50\ \mu s\ cm^{-1}$), suggesting that the transition to deeper flow paths may have started in limited locations (Figure 4c). Samples collected at the Wolverine Creek streamgage have EC and $\delta^{18}O$ signatures of the glacier outlet rather than the nonglacial streams (Figure 6c). Although the nonglacial areas are likely contributing to solute flux, stream chemistry appears to still be dominated by meltwater and the glacier drainage processes. This is supported by the diel EC and Q records, presumably reflecting daily pulsing and release of meltwater through the subglacial drainage network (Nanni

et al., 2019). Even though water is relatively dilute, the sheer quantity of water being exported and duration of the period makes this an important time for solute export (Hood & Berner, 2009).

We define the transition between P3 and P4 as both a switch from decreasing to increasing EC and the onset of late-season rains. Seasonal snow has mostly melted and ground thaw is at its greatest extent. Thus, it is likely that groundwater now supplies higher solute concentrations, driving EC upwards (Figures 2, 4d and 5). In nonglacial areas, we observe a distinct contribution from both shallow and deep groundwater, both of which have higher EC than meltwater (Figure 3d). Shallow groundwater is hypothesized to be confined to the shallow soils, which is typical of high latitude soils where an organic layer (O horizon) overlies mineral soils (Carey & Woo, 2001; Koch et al., 2017; Quinton & Marsh, 1999). What we consider deep groundwater likely represents deeper flow paths with longer residence times through mineral soils and/or the fractured bedrock (e.g., Toth, 1963, Table 1). Nonglacial stream chemistry spans the range between rain and shallow and deep groundwater source waters (Figure 4d).

Rain events occurring during P4 can influence total annual solute fluxes in two ways. First, fall rains produce high water flux and therefore high solute flux (Hindshaw et al., 2011; Krawczyk et al., 2003; Wadham et al., 1997). The second is that fall rain accesses different flow pathways than earlier season snowmelt and likely takes on a different geochemical signature. The largely chemostatic behavior we observe during this period ($b = -0.36$ in Table 2) is likely a function of flushing of both groundwater (Evans & Davies, 1998) and the subglacial drainage network (Denner et al., 1999). Samples collected at the glacier outlet span the range between meltwater and rain, indicating that rain does indeed reach the glacier bed (Figure 4d). Hydrologically, glaciers are important for short-term storage and release of precipitation, and as long-term supply of water during dry intervals during the late summer (Figure 2, Fountain & Walder, 1998). A large fall rain event that delivers a substantial water volume to the subglacial drainage network can cause a reorganization of channels and result in slower draining locations with longer residence times to connect to the faster draining system (Nanni et al., 2019; Rada & Schoof, 2018; Rutter, 2005; Wadham et al., 1997). When these areas are drained, they can increase total solute concentrations at the glacier outlet and contribute to observed outlet signatures (Figures 4d and 6d). During this period, both the glacier and nonglacierized areas make critical contributions to total solute fluxes (Figure 7).

In P4, nonglacial streams exhibit differences in average source water composition amongst each other (Figure 4d). The percentage of groundwater in nonglacial streams is much lower in 2017 than 2016 (16% ± 6% vs. 41% ± 9%, Figure 5). The higher precipitation inputs in 2017 likely reduced residence times and moved water to streams before taking on the groundwater signature (Kirchner & Neal, 2013; Ohrui & Mitchell, 1999). Higher precipitation in 2017 may have also promoted melt of any remaining nonglacier snow resulting in the higher snow/ice fraction (Marks et al., 1998; Musselman et al., 2018). The similar signature between years at the glacier outlet stream illustrates the stabilizing effect glaciers can have on the runoff regime (Figure 5; O'Neel et al., 2015).

Glacierized watersheds are particularly sensitive to the seasonality of precipitation (Fujita, 2008) and spring and fall temperatures (Oerlemans & Reichert, 2000). A change in the timing and form of precipitation can strongly impact snow accumulation and melt rates, with a long-term impact on geochemical signatures and fluxes. We observed strong relationships between Q and EC in periods 1 and 4, which are the shoulder seasons and are expected to see the most change (Littell et al., 2018; Mcafee et al., 2014). P1 is dominated by dilution of solutes, and therefore increased early season rain on its own may not result in increased solute export. However, warmer early season temperatures and more rain rather than snow may result in earlier shifts to other hydroclimatic periods with higher solute flux and increase the duration of the overall flow season. Solute export could increase in P4 when conditions are more chemostatic (Table 2). Fall 2017 provides a good example of the associated future hydro-chemical characteristics one might expect with this shift. In 2017, P4 precipitation was 1.5 times higher than in 2016 (514 vs. 760 mm). We observe stronger chemostasis and much larger aerial calcium flux in P4 during 2017 relative to 2016 (Figures 2 and 7, Table 2, Table S1 in Supporting Information S1). This suggests that, in the future, increased late season rain events may contribute more to total annual solute loads. Additionally, individual events appear more chemostatic than the entirety of P4 (Figure 2). An examination of EC-Q in individual events in future studies might provide more information on hydrologic process during this fairly long period.

At the very end of the record in early to mid-October of both seasons, Q decreased drastically and EC continued to increase (Figures 2a and 2b). Particularly in 2017, we observed a late October precipitation event with almost no Q response, suggesting that most of that storm was in the form of snow and the watershed was transitioning to winter (Figure 2b). This late season freeze-up interval could potentially be considered a fifth period. Unfortunately, because the EC sensor needs to be removed to avoid freezing damage, and we do not have any samples from that late in the season, we do not have sufficient data to characterize this time and choose to lump it with P4. However, this period could likely be identified and explored further in other locations with a record extending later in the year.

4.3. Integrating Geochemical Signatures Across Spatial Scales

Geochemical signatures at the Wolverine Creek streamgage and Nellie Juan River outlet are indicative of how larger watersheds and stream systems subsume some variability observed at smaller spatial scales. The Wolverine Creek streamgage is sited close to the glacier outlet and does not have much additional nonglacierized contributing area (11% of total watershed area) relative to the terminus. Because of this, the streamgage follows the source water dynamics of the glacier outlet samples very closely (Figure 6). The streamgage is most distinct from the glacier outlet in P2, the only time a streamgage sample falls outside 1 SD of glacier outlet samples. A stronger snowmelt signal at the streamgage is apparent, EC is 32 μs cm^{-1} at the streamgage while it was an average of 43 μs/cm at the glacier outlet (Figure 6b). At this time the glacier outlet still has high EC, reflecting the influence of the long residence time subglacial sources and groundwater, but this is diluted only 1.5 km downstream by rapid snowmelt in lower elevation nonglacier areas. The dominance of the glacier within the Wolverine Glacier watershed on outlet solute signatures resumes with the onset of P3 (Figure 6).

Wolverine glacier is rapidly losing mass and the terminus has retreated 1.5 km in the last 50 years (O'Neel et al., 2019). We expect that as the glacier continues to lose mass, thin, and retreat, its influence on the hydrograph and solute fluxes will diminish. We may possibly see the largest impacts in P4: as glacier covered area declines, the relative proportion of rain taking on the nonglacier signal will increase and help shift the overall outlet signature to be increasingly groundwater dominated (Figures 4d and 5a). Alternatively, the freshly exposed till will likely have high hydraulic conductivity (Ronayne et al., 2012) and therefore low average residence time, meaning the outlet signature may just be increasingly rain dominated in P4, as we observed in 2017 (Figure 6d).

At the broader scale, the Nellie Juan River has remarkably stable chemistry throughout the entire year (Figure 6). EC ranges 28–48 μS cm^{-1} across all samples ($n = 8$) collected at Nellie Juan River. In comparison EC ranged from 15 to 142 μS cm^{-1} at the Wolverine Creek streamgage ($n = 13$) and 5–62 μS cm^{-1} at the glacier outlet ($n = 49$). Similarly, the oxygen isotope signal only spans 2.5 per mil at Nellie Juan River while the range was 3.0 and 4.6 per mil at the streamgage and glacier outlet, respectively. The differences in seasonal stability between the Wolverine Glacier watershed and the larger Nellie Juan River watershed suggest that the large river system and greater watershed area acts as a low-pass filter on water chemistry (Shaman et al., 2004). There may be several contributing factors for the distinct stream chemistry at the Nellie Juan River outlet. First, the relative proportions of land cover are different. The larger Nellie Juan River watershed is 40% glacierized (as opposed to 60% in Wolverine Glacier watershed) and has much more area at low elevation dominated by forest, which has a distinctly different biogeochemical signature (Fellman et al., 2014; Hood & Berner, 2009; Hood & Scott, 2008). Second, the axis of the valley trends southwest-northeast. Watersheds on opposite sides of the valley have mostly north or south-facing aspects, which result in differential wind-loading and snow accumulation as well as available energy driving melt (McGrath et al., 2015). Differential snowmelt timing may integrate and smooth the meltwater to groundwater transition observed at the Nellie Juan River outlet. Finally, the Nellie Juan River has a large gravel alluvial aquifer and branching side channels particularly toward the outlet, which may result in a hyporheic zone with longer residence times and a large reservoir to mix and stabilize the geochemical signature (Kasahara & Wondzell, 2003). Though our data are not sufficient to resolve the relative influence of these factors, each are plausible contributions to the relative stability of the Nellie Juan River chemistry. This independent behavior at larger scales highlights the fact that understanding the watershed characteristics and distance from the glacier outlet strongly influences how we interpret source water contributions, processes, and flow paths setting water chemistry and solute flux estimations.

The stable stream chemistry we observe at the Nellie Juan outlet may indicate that the impacts of warming may be slightly buffered at the larger scale relative to the headwaters, such as the Wolverine Glacier watershed. Alternatively, the Nellie Juan watershed has a much greater area at low elevation than the Wolverine watershed, meaning it might be more susceptible to the increasing rain/snow transition

5. Conclusion

Our work in the Wolverine Glacier watershed identified four periods that may be broadly representative of common hydrologic behavior and climatic forcing in glacierized watersheds: initial snowmelt (P1), connection of the subglacial drainage network (P2), snow and ice melt (P3), and a rainy late season period (P4). This framework for classifying a melt season holds across 2 years of data despite variable climatic forcing between the two seasons. In both years, we observed clear differences in source water contributions across periods. Source waters have distinct solute concentrations and therefore influence the magnitude of solute flux from the watershed as sources change in relative provenance. Solute flux rates span an order of magnitude across the four periods, highlighting the need for careful consideration of how temporally discrete sampling informs extrapolation across spatial and temporal scales. Additionally, we observed early season dilution but more chemostatic behavior in late fall. The use of EC-Q relationships within this classification framework, coupled with predicted increases in late season precipitation as rain (Littell et al., 2018), suggests that we may see increased solute flux from fall rain events.

This research fills a critical gap by creating a conceptual framework for classifying time-varying surface water and associated solute source characteristics in partially glacierized watersheds. Classification of flow regimes in glacierized watersheds in particular has been applied to determine water sources and storages (e.g., Hannah et al., 2000; Swift et al., 2005), suspended sediment loading (e.g., Leggat et al., 2015; Orwin et al., 2010), and hydrograph prediction under continued glacier mass loss (e.g., Fleming & Clarke, 2005; Stahl & Moore, 2006). However, only a few studies have applied a classification scheme to determine time-varying solute fluxes over a melt season (Collins, 1999; Rasch et al., 2000). We suggest that this classification system could be expanded upon and used elsewhere to better contextualize solute export when sampling is temporally limited or to reanalyze previous data (e.g., Anderson et al., 1997; Axtmann & Stallard, 1995) to refine chemical weathering and solute flux estimates. Hydroclimatic periods could also be used to compare glacierized watersheds in space and time. Long-term records of EC, Q, and precipitation in a single watershed could be evaluated to compare how the duration and timing of the hydrologic periods change in response to climatic forcing and glacier mass loss. Additionally, we can compare locations with different geology, climate, or fractional glacier-covered area in order to classify or parse how climate and hydrologic routing are reflected in the streamflow and geochemical record. This study demonstrates the potential to use a classification scheme with easily collected continuous data to better constrain solute fluxes and understand how the retreat of glaciers will affect global geochemical cycles.

Data Availability Statement

Discharge and electrical conductivity data from the Wolverine Creek streamgage are publicly available and can be found the USGS National Water Information System database (Streamgage 15236900, Wolverine C nr Lawing AK; http://dx.doi.org/10.5066/F7P55KJN). Meteorological data from a mid-elevation station in the Wolverine Glacier watershed (Baker et al., 2019) and grab sample chemistry data (Koch et al., 2021) are available in USGS data releases.

Acknowledgments
The authors thank L. Sass, K. Myers, B. Smith, C. McNeil, J. Ostman, and S. Sawicki for help with field data collection, Alpine Air for helicopter support, and the Klein Lab and Applied Science and Engineering labs at the University of Alaska Anchorage and Deb Repert at the USGS lab in Boulder, CO, for water sample analysis. The authors would also like to thank Daniel Otto, Jamie Shanley, and Louis Sass for their helpful comments and suggestions during the preparation of this manuscript. This work was supported by an NSF Graduate Research Internship Program award and NSF Earth Sciences Post-Doctoral Fellowship awarded to Bergstrom. Any opinions, finding, conclusions, or recommendations expressed in the material are those of the authors and do not necessarily reflect the views of the National Science Foundation. U.S. Geological Survey support is granted by the Land Resources Mission Area, Climate Research and Development Program. Any use of trade, firm, or product names is for descriptive purposes only and does not imply endorsement by the U.S. Government.

References

Anderson, S. P., Drever, J. I., Frost, C. D., & Holden, P. (2000). Chemical weathering in the forefield of a retreating glacier. *Geochimica et Cosmochimica Acta*, *64*(7), 1173–1189.

Anderson, S. P., Drever, J. I., & Humphrey, N. F. (1997). Chemical weathering in glacial environments. *Geology*, *25*(5), 399–402. https://doi.org/10.1130/0091-7613(1997)025<0399:cwige>2.3.co;2

Arimitsu, M. L., Piatt, J. F., & Mueter, F. (2016). Influence of glacier runoff on ecosystem structure in Gulf of Alaska fjords. *Marine Ecology Progress Series*, *560*, 19–40. https://doi.org/10.3354/meps11888

Axtmann, E. V., & Stallard, R. F. (1995). Chemical weathering in the South Cascade Glacier basin, comparison of subglacial and extra-glacial weathering. *Biogeochemistry of Seasonally Snow-Covered Catchments*, *228*(228), 431–439.
Baker, E. H., Peitzsch, E., Sass, L. C., Miller, Z. M., & Whorton, E. N. (2019). *High altitude weather station data at USGS Benchmark Glaciers (version 1.0, July, 2019)*. https://doi.org/10.5066/P9EUXIPE
Barnes, R. T., Williams, M. W., Parman, J. N., Hill, K., & Caine, N. (2014). Thawing glacial and permafrost features contribute to nitrogen export from Green Lakes Valley, Colorado Front Range, USA. *Biogeochemistry*, *117*(2–3), 413–430. https://doi.org/10.1007/s10533-013-9886-5
Baron, J. S., Schmidt, T. M., & Hartman, M. D. (2009). Climate-induced changes in high elevation stream nitrate dynamics. *Global Change Biology*, *15*(7), 1777–1789. https://doi.org/10.1111/j.1365-2486.2009.01847.x
Beamer, J. P., Hill, D. F., McGrath, D., Arendt, A., & Kienholz, C. (2017). Hydrologic impacts of changes in climate and glacier extent in the Gulf of Alaska watershed. *Water Resources Research*, *53*(9), 7502–7520. https://doi.org/10.1002/2016WR020033
Bhatia, M. P., Das, S. B., Kujawinski, E. B., Henderson, P., Burke, A., & Charette, M. A. (2011). Seasonal evolution of water contributions to discharge from a Greenland outlet glacier: Insight from a new isotope-mixing model. *Journal of Glaciology*, *57*(205), 929–941. https://doi.org/10.3189/002214311798043861
Box, J. E., Colgan, W. T., Christensen, T. R., Schmidt, N. M., Lund, M., Parmentier, F. J. W., et al. (2019). Key indicators of Arctic climate change: 1971–2017. *Environmental Research Letters*, *14*(4). 045010. https://doi.org/10.1088/1748-9326/aafc1b
Box, J. E., Colgan, W. T., Wouters, B., Burgess, D. O., O'Neel, S., Thomson, L. I., & Mernild, S. H. (2018). Global sea-level contribution from Arctic land ice: 1971–2017. *Environmental Research Letters*, *13*(12). 125012. https://doi.org/10.1088/1748-9326/aaf2ed
Burns, D. A., McDonnell, J. J., Hooper, R. P., Peters, N. E., Freer, J. E., Kendall, C., & Beven, K. (2001). Quantifying contributions to storm runoff through end-member mixing analysis and hydrologic measurements at the Panola Mountain research watershed (Georgia, USA). *Hydrological Processes*, *15*(10), 1903–1924. https://doi.org/10.1002/hyp.246
Campbell, F. M. A., Nienow, P. W., & Purves, R. S. (2006). Role of the supraglacial snowpack in mediating meltwater delivery to the glacier system as inferred from dye tracer investigations. *Hydrological Processes*, *20*(4), 969–985. https://doi.org/10.1002/hyp.6115
Cantoni, C., Hopwood, M. J., Clarke, J. S., Chiggiato, J., Achterberg, E. P., & Cozzi, S. (2020). Glacial drivers of marine biogeochemistry indicate a future shift to more corrosive conditions in an Arctic fjord. *Journal of Geophysical Research: Biogeosciences*, *125*, e2020JG005633. https://doi.org/10.1029/2020JG005633
Carey, S. K. (2003). Dissolved organic carbon fluxes in a discontinuous permafrost subarctic alpine catchment. *Permafrost and Periglacial Processes*, *14*(2), 161–171. https://doi.org/10.1002/ppp.444
Carey, S. K., Boucher, J. L., & Duarte, C. M. (2013). Inferring groundwater contributions and pathways to streamflow during snowmelt over multiple years in a discontinuous permafrost subarctic environment (Yukon, Canada). *Hydrogeology Journal*, *21*(1), 67–77. https://doi.org/10.1007/s10040-012-0920-9
Carey, S. K., & Woo, M. K. (2001). Slope runoff processes and flow generation in a subarctic, subalpine catchment. *Journal of Hydrology*, *253*(1–4), 110–129. https://doi.org/10.1016/S0022-1694(01)00478-4
Cauvy-Fraunié, S., & Dangles, O. (2019). A global synthesis of biodiversity responses to glacier retreat. *Nature Ecology and Evolution*, *3*(12), 1675–1685. https://doi.org/10.1038/s41559-019-1042-8
Chapin, F. S. I., Trainor, S. F., Cochran, P., Huntington, H., Markon, C., McCammon, M., et al (2014). Alaska. Climate Change Impacts in the United States. *The Third National Climate Assessment*, 514–536. https://doi.org/10.7930/J00Z7150.On
Collins, D. N. (1999). Solute flux in meltwaters draining from a glacierized basin in the Karakoram mountains. *Hydrological Processes*, *13*(18), 3001–3015. https://doi.org/10.1002/(SICI)1099-1085(19991230)13:18<3001::AID-HYP15>3.0.CO;2-N
Cuffey, K. M., & Paterson, W. S. B. (2010). *The physics of glaciers*. Academic Press.
Curran, J. H., & Biles, F. E. (2021). Identification of seasonal streamflow regimes and streamflow drivers for daily and peak flows in Alaska. *Water Resources Research*, *57*(2), 1–21.
Dahlke, H. E., Lyon, S. W., Jansson, P., Karlin, T., & Rosqvist, G. (2014). Isotopic investigation of runoff generation in a glacierized catchment in northern Sweden. *Hydrological Processes*, *28*(3), 1383–1398. https://doi.org/10.1029/2020wr028425
Dansgaard, W. (1964). Stable isotopes in precipitation. *Tellus*, *16*(4), 436–468. https://doi.org/10.3402/tellusa.v16i4.8993
Denner, J. C., Lawson, D. E., Larson, G. J., Evenson, E. B., Alley, R. B., Strasser, J. C., & Kopczynski, S. (1999). Seasonal variability in hydrologic-system response to intense rain events, Matanuska Glacier, Alaska, U.S.A. *Annals of Glaciology*, *28*, 267–271.
Déry, S. J., Hernández-Henríquez, M. A., Burford, J. E., & Wood, E. F. (2009). Observational evidence of an intensifying hydrological cycle in northern Canada. *Geophysical Research Letters*, *36*(13).
Dessert, C., Dupré, B., Gaillardet, J., François, L. M., & Allegre, C. J. (2003). Basalt weathering laws and the impact of basalt weathering on the global carbon cycle. *Chemical Geology*, *202*(3–4), 257–273.
Dolan, D. M., Yui, A. K., & Geist, R. D. (1981). Evaluation of river load estimation methods for total phosphorus. *Journal of Great Lakes Research*, *7*(3), 207–214.
Dzikowski, M., & Jobard, S. (2012). Mixing law versus discharge and electrical conductivity relationships: Application to an alpine proglacial stream. *Hydrological Processes*, *26*(18), 2724–2732. https://doi.org/10.1002/hyp.8366
Evans, C., & Davies, T. D. (1998). Causes of concentration/discharge hysteresis and its potential as a tool for analysis of episode hydrochemistry. *Water Resources Research*, *34*(1), 129–137. https://doi.org/10.1029/2009gl038852
Evans, S. G., Ge, S., Voss, C. I., & Molotch, N. P. (2018). The role of frozen soil in groundwater discharge predictions for warming Alpine Watersheds. *Water Resources Research*, *54*, 1599–1615. https://doi.org/10.1016/s0380-1330(81)72047-1
Evans, W., Mathis, J. T., & Cross, J. N. (2014). Calcium carbonate corrosivity in an Alaskan inland sea. *Biogeosciences*, *11*(2), 365–379.
Fairchild, I. J., Killawee, J. A., Sharp, M. J., Spiro, B., Hubbard, B., Lorrain, R. D., & Tison, J. L. (1999). Solute generation and transfer from a chemically reactive alpine glacial-proglacial system. *Earth Surface Processes and Landforms*, *24*(13), 1189–1211. https://doi.org/10.1002/(SICI)1096-9837(199912)24:13<1189::AID-ESP31>3.0.CO;2-P
Fellman, J. B., Hood, E., Dryer, W., & Pyare, S. (2015). Stream physical characteristics impact habitat quality for pacific salmon in two temperate coastal watersheds. *PLoS One*, *10*(7), 1–16. https://doi.org/10.5194/bg-11-365-2014
Fellman, J. B., Hood, E., Spencer, R. G. M., Stubbins, A., & Raymond, P. A. (2014). Watershed glacier coverage influences dissolved organic matter biogeochemistry in coastal watersheds of southeast Alaska. *Ecosystems*, *17*(6), 1014–1025. https://doi.org/10.1002/2017wr022098
Fleming, S. W., & Clarke, G. K. C. (2005). Attenuation of high-frequency interannual streamflow variability by watershed glacial cover. *Journal of Hydraulic Engineering*, *131*(7), 615–618. https://doi.org/10.1061/(ASCE)0733-9429(2005)131
Fountain, A. G., & Tangborn, W. V. (1985). The effect of glaciers on streamflow variations. *Water Resources Research*, *21*(4), 579–586. https://doi.org/10.1029/WR021i004p00579

Fountain, A. G., & Walder, J. S. (1998). Water flow through temperate glaciers. *Reviews of Geophysics*, *36*(3), 299–328. https://doi.org/10.1029/97RG03579

Fujita, K. (2008). Influence of precipitation seasonality on glacier mass balance and its sensitivity to climate change. *Annals of Glaciology*, *48*, 88–92. https://doi.org/10.1061/(asce)0733-9429(2005)131:7(615)

Gat, J. R., & Dansgaard, W. (1972). Stable isotope survey of the fresh water occurrences in Israel and the northern Jordan Rift Valley. *Journal of Hydrology*, *16*, 177–212.

Godsey, S., Kirchner, J. W., & Clow, D. W. (2009). Concentration - Discharge relationships reflect chemostatic characteristics of US catchments. *Hydrological Processes*, *23*, 1844–1864. https://doi.org/10.1002/hyp.7315

Graly, J., Harrington, J., & Humphrey, N. (2017). Combined diurnal variations of discharge and hydrochemistry of the Isunnguata Sermia outlet, Greenland Ice Sheet. *The Cryosphere*, *11*(3), 1131–1140.

Hallet, B., Hunter, L., & Bogen, J. (1996). Rates of erosion and sediment evacuation by glaciers: A review of field data and their implications. *Global and Planetary Change*, *12*(1–4), 213–235. https://doi.org/10.1016/0022-1694(72)90052-2

Hannah, D. M., Smith, B. P. G., Gurnell, A. M., & McGregor, G. R. (2000). An approach to hydrograph classification. *Hydrological Processes*, *14*(2), 317–338. https://doi.org/10.1002/(SICI)1099-1085(20000215)142<317::AID-HYP929>3.0.CO;2-T

Harper, J. T., Humphrey, N., & Greenwood, M. C. (2002). Basal conditions and glacier motion during the winter/spring transition, Worthington Glacier, Alaska, USA. *Journal of Glaciology*, *48*(160), 42–50.

Hawkings, J., Wadham, J. L., Tranter, M., Lawson, E. C., Sole, A., Cowton, T., et al (2015). The effect of warming climate on nutrient and solute export from the Greenland Ice Sheet. *Geochemical Perspectives Letters*, 94–104. https://doi.org/10.7185/geochemlet.1510

Herman, F., Seward, D., Valla, P., et al (2013). Worldwide acceleration of mountain erosion under a cooling climate. *Nature*, *504*, 423–426. https://doi.org/10.1038/nature12877

Hindshaw, R. S., Tipper, E. T., Reynolds, B. C., Lemarchand, E., Wiederhold, J. G., Magnusson, J., et al (2011). Hydrological control of stream water chemistry in a glacial catchment (Damma Glacier, Switzerland). *Chemical Geology*, *285*(1–4), 215–230. https://doi.org/10.1002/(sici)1099-1085(20000215)14:2<317::aid-hyp929>3.0.co;2-t

Hodgkins, R. (2001). Seasonal evolution of meltwater generation, storage and discharge at a non-temperate glacier in Svalbard. *Hydrological Processes*, *15*(3), 441–460. https://doi.org/10.3189/172756502781831629

Hodson, A., Porter, P., Lowe, A., & Mumford, P. (2002). Chemical denudation and silicate weathering in Himalayan glacier basins: Batura Glacier, Pakistan. *Journal of Hydrology*, *262*(1–4), 193–208. https://doi.org/10.1016/S0022-1694(02)00036-7

Hodson, A, Tranter, M., Gurnell, A., Clark, M., & Hagen, J. O. (2002). The hydrochemistry of Bayelva, a high Arctic proglacial stream in Svalbard. *Journal of Hydrology*, *257*(1–4), 91–114. https://doi.org/10.1016/S0022-1694(01)00543-1

Hood, E., Battin, T. J., Fellman, J., O'Neel, S., & Spencer, R. G. M. (2015). Storage and release of organic carbon from glaciers and ice sheets. *Nature Geoscience*, *8*(2), 91–96. https://doi.org/10.1038/ngeo2331

Hood, E., & Berner, L. (2009). Effects of changing glacial coverage on the physical and biogeochemical properties of coastal streams in southeastern Alaska. *Journal of Geophysical Research: Biogeosciences*, *114*(3), 1–10. https://doi.org/10.1029/2009JG000971

Hood, E., Fellman, J. B., Spencer, R. G. M., Hernes, P. J., Edwards, R., D'Amore, D., & Scott, D. T. (2009). Glaciers as a source of ancient and labile organic matter to the marine environment. *Nature*, *462*(7276), 1044–1047. https://doi.org/10.1038/nature08580

Hood, E., & Scott, D. T. (2008). Riverine organic matter and nutrients in southeast Alaska affected by glacial coverage. *Nature Geoscience*, *1*(9), 583–587. https://doi.org/10.1038/ngeo280

Horton, P., Schaefli, B., Mezghani, A., Hingray, B., & Musy, A. (2006). Assessment of climate-change impacts on alpine discharge regimes with climate model uncertainty. *Hydrological Processes*, *20*(10), 2091–2109. https://doi.org/10.1002/hyp.6197

Huss, M., & Hock, R. (2015). A new model for global glacier change and sea-level rise. *Frontiers of Earth Science*, *3*, 1–22. https://doi.org/10.3389/feart.2015.00054

Ibarra, D. E., Moon, S., Caves, J. K., et al. (2017). Concentration–discharge patterns of weathering products from global rivers. *Acta Geochimica*, *36*, 405–409. https://doi.org/10.1007/s11631-017-0177-z

Jansson, P., Hock, R., & Schneider, T. (2003). The concept of glacier storage: A review. *Journal of Hydrology*, *282*(1–4), 116–129. https://doi.org/10.1016/S0022-1694(03)00258-0

Kamb, B., Raymond, C. F., Harrison, W. D., Engelhardt, H., Echelmeyer, K. A., Humphrey, N., et al (1985). Glacier surge mechanism: 1982–1983 surge of variegated glacier, Alaska. *Science*, *227*(4686), 469–479. https://doi.org/10.1126/science.227.4686.469

Kasahara, T., & Wondzell, S. M. (2003). Geomorphic controls on hyporheic exchange flow in mountain streams. *Water Resources Research*, *39*(1), 1–14. https://doi.org/10.1029/2002WR001386

Kirchner, J. W., & Neal, C. (2013). Universal fractal scaling in stream chemistry and its implications for solute transport and water quality trend detection. *Proceedings of the National Academy of Sciences*, *110*(30), 12213–12218. https://doi.org/10.1073/pnas.1304328110

Koch, J. C., Baker, E. H., Bergstrom, A., & O'Neel, S. (2021). *Geochemistry of water sources in the Wolverine Glacier Watershed. Alaska in 2016 and 2017*. U.S. Geological Survey. https://doi.org/10.5066/P9LLXNAX

Koch, J. C., Kikuchi, C. P., Wickland, K. P., & Schuster, P. (2014). Runoff sources and flow paths in a partially burned, upland boreal catchment underlain by permafrost. *Water Resources Research*, *50*(10), 8141–8158. https://doi.org/10.1002/2014WR015586

Koch, J. C., McKnight, D. M., & Baeseman, J. L. (2010). Effect of unsteady flow on nitrate loss in an oligotrophic, glacial meltwater stream. *Journal of Geophysical Research: Biogeosciences*, *115*(1), 1–15. https://doi.org/10.1029/2009JG001030

Koch, J. C., Runkel, R. L., Striegl, R., & McKnight, D. M. (2013). Hydrologic controls on the transport and cycling of carbon and nitrogen in a boreal catchment underlain by continuous permafrost. *Journal of Geophysical Research: Biogeosciences*, *118*(2), 698–712. https://doi.org/10.1002/jgrg.20058

Koch, J. C., Toohey, R. C., & Reeves, D. M. (2017). Tracer-based evidence of heterogeneity in subsurface flow and storage within a boreal hillslope. *Hydrological Processes*, *31*(13), 2453–2463. https://doi.org/10.1002/hyp.11205

Krawczyk, W. E., Lefauconnier, B., & Pettersson, L. (2003). Chemical denudation rates in the Bayelva Catchment, Svalbard, in the Fall of 2000. *Physics and Chemistry of the Earth*, *28*, 1257–1271. https://doi.org/10.1016/j.pce.2003.08.054

Lachniet, M. S., Lawson, D. E., Stephen, H., Sloat, A. R., & Patterson, W. P. (2016). Isoscapes of $\delta^{18}O$ and $\delta^{2}H$ reveal climatic forcings on Alaska and Yukon precipitation. *Water Resources Research*, *52*, 6575–6586. https://doi.org/10.1002/2014WR016618

Leggat, M. S., Owens, P. N., Stott, T. A., Forrester, B. J., Déry, S. J., & Menounos, B. (2015). Hydro-meteorological drivers and sources of suspended sediment flux in the pro-glacial zone of the retreating Castle Creek Glacier, Cariboo Mountains, British Columbia, Canada. *Earth Surface Processes and Landforms*, *40*(11), 1542–1559. https://doi.org/10.1002/esp.3755

Likens, G. E., Bormann, F. H., Johnson, N. M., & Pierce, R. S. (1967). The calcium, magnesium, potassium, and sodium budgets for a small forested ecosystem. *Ecology*, *48*(5), 772–785.

Liljedahl, A. K., Gädeke, A., O'Neel, S., Gatesman, T. A., & Douglas, T. A. (2017). Glacierized headwater streams as aquifer recharge corridors, subarctic Alaska. *Geophysical Research Letters*, *44*(13), 6876–6885. https://doi.org/10.1016/j.pce.2003.08.054

Littell, J. S., McAfee, S. A., & Hayrd, G. D. (2018). Alaska snowpack response to climate change: Statewide snowfall equivalent and snowpack water scenarios. *Water*, *10*(5), 668.

Liu, F., Williams, M. W., & Caine, N. (2004). Source waters and flow paths in an alpine catchment, Colorado Front Range, United States. *Water Resources Research*, *40*(9), 1–16. https://doi.org/10.1029/2004WR003076

Maclean, R., Oswood, M. W., Irons, J. G., & Mcdowell, W. H. (1999). The effect of permafrost on stream biogeochemistry: A case study of two streams in the Alaskan (USA) Taiga. *Biogeochemistry*, *47*(3), 239–267. https://doi.org/10.1007/BF00992909

Maher, K. (2011). The role of fluid residence time and topographic scales in determining chemical fluxes from landscapes. *Earth and Planetary Science Letters*, *312*(1–2), 48–58.

Malard, F., Tockner, K., & Ward, J. V. (1999). Shifting dominance of subcatchment water sources and flow paths in a glacial floodplain, Val Roseg, Switzerland. *Arctic Antarctic and Alpine Research*, *31*(2), 135–150. https://doi.org/10.1080/15230430.1999.12003291

Marks, D., Kimball, J., Tingey, D., & Link, T. (1998). The sensitivity of snowmelt processes to climate conditions and forest cover during rain-on-snow: A case study of the 1996 Pacific Northwest flood. *Hydrological Processes*, *12*(10–11), 1569–1587.

Marzeion, B., Hock, R., Anderson, B., Bliss, A., Champollion, N., Fujita, K., et al (2020). Partitioning the uncertainty of ensemble projections of global glacier mass change. *Earth's Future*, *8*(7), 1–25. https://doi.org/10.3390/w10050668

Mcafee, S. A., Walsh, J. E., & Rupp, T. S. (2014). Statistically downscaled projections of snow/rain partitioning for Alaska. *Hydrological Processes*, *28*(12), 3930–3946. https://doi.org/10.1002/hyp.9934

McGlynn, B. L., & McDonnell, J. J. (2003). Quantifying the relative contributions of riparian and hillslope zones to catchment runoff. *Water Resources Research*, *39*, 1310. https://doi.org/10.1029/2003WR002091

McGlynn, B. L., Mcdonnell, J. J., Shanley, J. B., & Kendall, C. (1999). Riparian zone flowpath dynamics during snowmelt in a small headwater catchment. *Journal of Hydrology*, *222*, 75–92.

McGovern, M., Pavlov, A. K., Deininger, A., Granskog, M. A., Leu, E., Søreide, J. E., & Poste, A. E. (2020). Terrestrial Inputs Drive Seasonality in Organic Matter and Nutrient Biogeochemistry in a High Arctic Fjord System (Isfjorden, Svalbard). *Frontiers in Marine Science*, *7*, 747

McGrath, D., Sass, L., O'Neel, S., Arendt, A., & Kienholz, C. (2017). Hypsometric control on glacier mass balance sensitivity in Alaska and northwest Canada. *Earth's Future*, *5*(3), 324–336. https://doi.org/10.1002/2016EF000479

McGrath, D., Sass, L. C., O'Neel, S., Arendt, A. A., Wolken, G. J., Gusmeroli, A., et al (2015). End-of-winter snow depth variability on glaciers in Alaska. *Journal of Geophysical Research: Earth Surface*, *120*, 1530–1550. https://doi.org/10.1002/(sici)1099-1085(199808/09)12:10/11<1569::aid-hyp682>3.0.co;2-l

McKnight, D. M., Cozzetto, K., Cullis, J. D. S., Gooseff, M., Jaros, C., Koch, J. C., et al (2015). A revised model formicrobially induced calcite precipitation: Improvements and new insights based on recent experiments. *Water Resources Research*, *51*, 6725–6738. https://doi.org/10.1002/2015WR017618.Received

Meier, M. F., Tangborn, W. V., Mayo, L. R., & Post, A. (1971). Combined ice and water balances of Gulkana and Wolverine Glaciers, Alaska, and South Cascade Glacier. Washington, 1965 and 1966 hydrologic years. Geological Survey Professional Paper. 715-A. https://doi.org/10.1017/S001675680003987X

Milner, A. M., Khamis, K., Battin, T. J., Brittain, J. E., Barrand, N. E., Füreder, L., et al (2017). Glacier shrinkage driving global changes in downstream systems. *Proceedings of the National Academy of Sciences of the United States of America*, *114*(37), 9770–9778. https://doi.org/10.1073/pnas.1619807114

Musselman, K. N., Clark, M. P., Liu, C., Ikeda, K., & Rasmussen, R. (2017). Slower snowmelt in a warmer world. *Nature Climate Change*, *7*(3), 214–219. https://doi.org/10.1016/s0022-1694(99)00102-x

Musselman, K. N., Lehner, F., Ikeda, K., et al. (2018). Projected increases and shifts in rain-on-snow flood risk over western North America. *Nature Climate Change*, *8*, 808–812. https://doi.org/10.1038/s41558-018-0236-4

Nanni, U., Gimbert, F., Vincent, C., Gräff, D., Walter, F., Piard, L., & Moreau, L. (2019). Seasonal and diurnal dynamics of subglacial channels: Observations beneath an Alpine Glacier. *The Cryosphere Discussions*, *20*, 1–31. https://doi.org/10.3389/fmars.2020.542563

Nienow, P., Sharp, M. J., & Willis, I. (1998). Seasonal changes in the morphology of the subglacial drainage system, Haut Glacier d'Arolla, Switzerland. *Earth Surface Processes and Landforms*, *23*(9), 825–843. https://doi.org/10.1002/(SICI)1096-9837(199809)23:9<825::AID-ESP893>3.0.CO;2–2

Oerlemans, J., & Reichert, B. K. (2000). Relating glacier mass balance to meteorological data by using a seasonal sensitivity characteristic. *Journal of Glaciology*, *46*(152), 1–6. https://doi.org/10.3189/172756500781833269

Ohrui, K., & Mitchell, M. J. (1999). Hydrological flow paths controlling stream chemistry in Japanese forested watersheds. *Hydrological Processes*, *13*(6), 877–888. https://doi.org/10.1002/(SICI)1099-1085(19990430)13:6<877::AID-HYP762>3.0.CO;2-E

Olden, J. D., Kennard, M. J., & Pusey, B. J. (2012). A framework for hydrologic classification with a review of methodologies and applications in ecohydrology. *Ecohydrology*, *5*(4), 503–518.

O'Neel, S., Hood, E., Arendt, A., & Sass, L. (2014). Assessing streamflow sensitivity to variations in glacier mass balance. *Climatic Change*, *123*(2), 329–341. https://doi.org/10.1007/s10584-013-1042-

O'Neel, S., Hood, E., Bidlack, A. L., Fleming, S. W., Arimitsu, M. L., Arendt, A., et al (2015). Icefield-to-ocean linkages across the northern pacific coastal temperate rainforest ecosystem. *BioScience*, *65*(5), 499–512. https://doi.org/10.1093/biosci/biv027

O'Neel, S., McNeil, C., Sass, L. C., Florentine, C., Baker, E. H., Peitzsch, E., et al (2019). Reanalysis of the US Geological Survey Benchmark Glaciers: Long-term insight into climate forcing of glacier mass balance. *Journal of Glaciology*, *65*(253), 850–866. https://doi.org/10.1017/jog.2019.66

Orwin, J. F., Guggenmos, M. R., & Holland, P. G. (2010). Changes in suspended sediment to solute yield ratios from an alpine basin during the transition to winter, southern Alps, New zealand. *Geografiska Annaler—Series A: Physical Geography*, *92*(2), 247–261. https://doi.org/10.1002/(sici)1096-9837(199809)23:9<825::aid-esp893>3.0.co;2-2

Patten, D. J. V. (2000). Soil Survey of Lower Kenai Peninsula Area, Alaska.

Quinton, W. L., & Marsh, P. (1999). A conceptual framework for runoff generation in a permafrost environment. *Hydrological Processes*, *13*(16), 2563–2581. https://doi.org/10.1002/(SICI)1099-1085(199911)13:16<2563::AID-HYP942>3.0.CO;2-D

Rada, C., & Schoof, C. (2018). Channelized, distributed, and disconnected: Subglacial drainage under a valley glacier in the Yukon. *The Cryosphere*, *12*(8), 2609–2636. https://doi.org/10.5194/tc-12-2609-2018

Rasch, M., Elberling, B., Jakobsen, B. H., & Hasholt, B. (2000). High-Resolution Measurements of Water Discharge, Sediment, and Solute Transport in the River Zackenbergelven, Northeast Greenland. *Arctic Antarctic and Alpine Research*, *32*(3), 336–345. https://doi.org/10.1080/15230430.2000.12003372

Raymond, P. A., McClelland, J. W., Holmes, R. M., Zhulidov, A. V., Mull, K., Peterson, B. J., et al. (2007). Flux and age of dissolved organic carbon exported to the Arctic Ocean: A carbon isotopic study of the five largest arctic rivers. *Global Biogeochemical Cycles*, *21*(4). https://doi.org/10.1029/2007GB002934

Ronayne, M. J., Houghton, T. B., & Stednick, J. D. (2012). Field characterization of hydraulic conductivity in a heterogeneous alpine glacial till. *Journal of Hydrology*, *458*, 103–109.

Ross, M. R. V., Nippgen, F., Hassett, B. A., McGlynn, B. L., & Bernhardt, E. S. (2018). Pyrite oxidation drives exceptionally high weathering rates and geologic CO_2 release in mountaintop-mined landscapes. *Global Biogeochemical Cycles*, *32*, 1182–1194. https://doi.org/10.1029/2017GB005798

Rutter, N. J. (2005). Impact of subglacial hydrology on the release of water from temporary storage in an Alpine glacier. *Annals of Glaciology*, *40*, 67–75.

Saros, J. E., Rose, K. C., Clow, D. W., Stephens, V. C., Nurse, A. B., Arnett, H. A., et al. (2010). Melting alpine glaciers enrich high-elevation lakes with reactive nitrogen. *Environmental Science and Technology*, *44*(13), 4891–4896. https://doi.org/10.1021/es100147j

Sergeant, C. J., Falke, J. A., Bellmore, R. A., Bellmore, J. R., & Crumley, R. L. (2020). A classification of streamflow patterns across the coastal Gulf of Alaska. *Water Resources Research*, *56*(2).e2019WR026127

Shaman, J., Stieglitz, M., & Burns, D. (2004). Are big basins just the sum of small catchments? *Hydrological Processes*, *18*(16), 3195–3206. https://doi.org/10.1002/hyp.5739

Singh, P., Kumar, A., & Kishore, N. (2011). Meltwater storage and delaying characteristics of Gangotri Glacier (Indian Himalayas) during ablation season. *Hydrological Processes*, *25*(2), 159–166. https://doi.org/10.1002/hyp.7828

Singley, J. G., Wlostowski, A. N., Bergstrom, A., Sokol, E. R., Torrens, C. L., Jaros, C., et al (2017). Characterizing hyporheic exchange processes using high- frequency electrical conductivity-discharge relationships on subhourly to interannual timescales. *Water Resources Research*, *53*, 4124–4141. https://doi.org/10.1002/2016WR019739

Spence, C., & Woo, M. K. (2003). Hydrology of subarctic Canadian shield: Soil-filled valleys. *Journal of Hydrology*, *279*(1–4), 151–166. https://doi.org/10.1016/j.jhydrol.2012.06.036

Stahl, K., & Moore, R. D. (2006). Influence of watershed glacier coverage on summer streamflow in British Columbia, Canada. *Water Resources Research*, *42*(6), 2–6. https://doi.org/10.1029/2006WR005022

Statham, P. J., Skidmore, M., & Tranter, M. (2008). Inputs of glacially derived dissolved and colloidal iron to the coastal ocean and implications for primary productivity. *Global Biogeochemical Cycles*, *22*(3).

Stewart, M. K. (1975). Stable isotope fractionation doe to evaporation and isotopic exchange of falling waterdrops: Applications to atmospheric processes and evaporation of lakes. *Journal of Geophysical Research*, *80*(9), 1133–1146.

Stubbins, A., Hood, E., Raymond, P. A., Aiken, G. R., Sleighter, R. L., Hernes, P. J., et al (2012). Anthropogenic aerosols as a source of ancient dissolved organic matter in glaciers. *Nature Geoscience*, *5*(3), 198–201. https://doi.org/10.1038/ngeo1403

Suchet, P. A., & Probst, J. L. (1995). A global model for present-day atmospheric/soil CO_2 consumption by chemical erosion of continental rocks (GEM-CO_2). *Tellus B: Chemical and Physical Meteorology*, *47*, 273–280. https://doi.org/10.1034/j.1600-0889.47.issue1.23.x

Swift, D. A., Nienow, P. W., Hoey, T. B., & Mair, D. W. F. (2005). Seasonal evolution of runoff from Haut Glacier d'Arolla, Switzerland and implications for glacial geomorphic processes. *Journal of Hydrology*, *309*(1–4), 133–148. https://doi.org/10.1016/j.jhydrol.20

Torres, M. A., Moosdorf, N., Hartmann, J., Adkins, J. F., & West, A. J. (2017). Glacial weathering, sulfide oxidation, and global carbon cycle feedbacks. *Proceedings of the National Academy of Sciences*, *114*(33):8716–8721. https://doi.org/10.1073/pnas.1702953114

Toth, J. (1963). A theoretical analysis of groundwater flow in small drainage basins 1 of phe low order stream and having similar the outlet of lowest impounded body of a relatively. *Journal of Geophysical Research*, *68*(16), 4795–4812.

Tranter, M., Huybrechts, P., Munhoven, G., Sharp, M. J., Brown, G. H., Jones, I. W., & Wadham, J. L. (2002). Direct effect of ice sheets on terrestrial bicarbonate, sulphate and base cation fluxes during the last glacial cycle: Minimal impact on atmospheric CO2 concentrations. *Chemical Geology*, *190*(1–4), 33–44.

Tranter, M., Sharp, M. J., Brown, G. H., Willis, I. C., Hubbard, B., Nielsen, M. K., et al (1997). Variability in the chemical composition of in situ subglacial meltwaters. *Hydrological Processes*, *11*, 59–77.

Valentin, M. M., Hogue, T. S., & Hay, L. E. (2018). Hydrologic regime changes in a high-latitude glacierized watershed under future climate conditions. *Water*, *10*(2), 128.

Van Beusekom, A. E. E., O'Neel, S., March, R. S., Sass, L., & Cox, L. H. H. (2010). *Re-analysis of Alaskan benchmark glacier mass-balance data using the index method Scientific Investigations Report 2010–5247*. US Geological Survey.

Wadham, J. L., Hodson, A. J., Tranter, M., & Dowdeswell, J. A. (1997). The rate of chemical weathering beneath a quiescent, surge-type, polythermal-based glacier, southern Spitsbergen, Svalbard. *Annals of Glaciology*, *24*, 27–31. https://doi.org/10.1029/2007gb003106

Werder, M. A., Hewitt, I. J., Schoof, C. G., & Flowers, G. E. (2013). Modeling channelized and distributed subglacial drainage in two dimensions. *Journal of Geophysical Research: Earth Surface*, *118*(4), 2140–2158. https://doi.org/10.1029/jc080i009p01133

Williams, M. W., Seibold, C., & Chowanski, K. (2009). Storage and release of solutes from a subalpine seasonal snowpack: Soil and stream water response, Niwot Ridge, Colorado. *Biogeochemistry*, *95*(1), 77–94. https://doi.org/10.1007/s10533-009-9288-x

Wilson, F. H., Hults, C. P., Labay, K. A., & Shew, N. (2008). *Digital data for the reconnaissance geologic map for Prince William Sound and the Kenai Peninsula*. U.S. Geological Survey Open-File Report 2008–1002.

Yde, J. C., Tvis Knudsen, N., & Nielsen, O. B. (2005). Glacier hydrochemistry, solute provenance, and chemical denudation at a surge-type glacier in Kuannersuit Kuussuat, Disko Island, West Greenland. *Journal of Hydrology*, *300*(1–4), 172–187. https://doi.org/10.1016/j.jhydrol.20

Zemp, M., Frey, H., Gärtner-Roer, I., Nussbaumer, S. U., Hoelzle, M., Paul, F., et al (2015). Historically unprecedented global glacier decline in the early 21st century. *Journal of Glaciology*, *61*(228), 745–762. https://doi.org/10.3189/2015JoG15J017

Zemp, M., Huss, M., Thibert, E., Eckert, N., McNabb, R., Huber, J., et al (2019). Global glacier mass changes and their contributions to sea-level rise from 1961 to 2016. *Nature*, *568*(7752), 382–386. https://doi.org/10.1038/s41586-019-1071-0

Zhu, P., & Macdougall, J. D. (1998). Calcium isotopes in the marine environment and the oceanic calcium cycle. *Geochimica et Cosmochimica Acta*, *62*(10), 1691–1698.

Ziemen, F. A., Hock, R., Aschwanden, A., Khroulev, C., Kienholz, C., Melkonian, A., & Zhang, J. (2016). Modeling the evolution of the Juneau Icefield between 1971 and 2100 using the Parallel Ice Sheet Model (PISM). *Journal of Glaciology*, *62*(231), 199–214. https://doi.org/10.1017/jog.2016.13

Zuecco, G., Carturan, L., De Blasi, F., Seppi, R., Zanoner, T., Penna, D., et al (2018). Understanding hydrological processes in glacierized catchments: Evidence and implications of highly-variable isotopic and electrical conductivity data. *Hydrological Processes*, *33*(5). 816-832. https://doi.org/10.1016/s0009-2541(02)00109-2